FINAL REPORT

FOR THE PERIOD

October 1, 1963 to September 30, 1964

THE STUDY OF BASE HEATING BY RADIATION FROM EXHAUST GASES

by

W. H. Giedt
C. L. Tien
R. N. Meroney
M. M. Abu-Romia
L. S. Wang

University of California at Berkeley
Aeronautical Sciences Laboratory

October 20, 1964

Prepared for
George C. Marshall Space Flight Center, NASA,
Huntsville, Alabama

Under Contract No. NAS 8-850

FACULTY INVESTIGATORS:

W. H. GIEDT, Professor of Aeronautical Sciences
C. L. TIEN, Associate Professor of Mechanical Engineering

SUMMARY

This investigation of radiation from rocket-engine gases was initiated with analytical studies of the radiative energy transfer from an exhaust plume to the base region of a booster vehicle. Attention was first devoted to semi-infinite cylindrical and infinite conical gas bodies of uniform temperature and composition. The procedures developed are described in the first section of the present report. Also included are results for the semi-infinite cylindrical plume. These are in the form of the spectral apparent emissivity of the gas body as viewed from the bore region.

The relationship for the spectral apparent emissivity is in integral form. An analytical expression was obtained for semi-infinite cylindrical gas bodies of small absorption coefficient. For other cases results were obtained by numerical integrations. Curves for the spectral apparent emissivity are presented as a function of the radial distance in the base plane of the gas body. The height of the engine nozzle and the spectral absorption coefficient appear as parameters.

An approximate method of calculating the total apparent emissivity based on the mean path length concept was developed. This is illustrated by applying the method to the calculation of the total apparent emissivity of semi-infinite cylindrical gas bodies composed of CO_2 at 2500 ^{o}R and H_2O at 2000 ^{o}R.

These total apparent emissivity calculations called attention to the need for complete knowledge of all the infrared absorption characteristics of combustion products. Since these are not available, an experimental

program was undertaken to study systematically the infrared spectral characteristics of a number of common combustion products under a variety of accurately known thermodynamic and optical conditions.

The second section of this report reviews the considerations which led to the construction of a high-temperature furnace system for infrared spectral absorption studies up to temperature of about 2000 ^{o}K. The apparatus consists of a graphite resistance furnace with an inner ceramic tube for containment of high-temperature gases. Data for the fundamental band of CO at temperatures of 300 ^{o}K and 1800 ^{o}K and at pressures from 0.25 to 3.0 atmospheres are presented. Comparison with existing experimental data shows agreement within 15 per cent. Future experimental plans include CO measurements at intermediate and possibly higher temperatures and similar measurement of CO_2 and H_2O.

THE STUDY OF BASE HEATING BY RADIATION FROM EXHAUST GASES

PLUME RADIATION STUDIES

Calculation of the Rocket Engine Exhaust Plume Radiation to the Base Region

This section describes the results of analyses of the radiative energy transfer from rocket exhaust plumes to the base regions based on idealized physical models. Consider a semi-infinite cylindrical gas body of uniform temperature and composition, emitting and absorbing radiative energy as shown in Fig. 1. The gas body is separated from a differential area dA by a non-absorbing medium. No scattering of radiation exists in the system. The spectral apparent emissivity, defined as the ratio of the radiative energy flux to that of a black body at the same temperature, is given as,[1]

$$\epsilon_\lambda = \frac{1}{\pi}\int_\beta \int_\phi (1-e^{-A_\lambda S}) \sin\beta \cos\beta \, d\beta \, d\phi \qquad (1)$$

where $A_\lambda = a_\lambda r_o$, $S = (s/r_o)$, a_λ is the linear spectral absorption coefficient, r_o is the radius of the cylindrical body, and thepath length s is a function of the height of shielding h, the radial distance in the base plane r, the azimuth angle ϕ and the polar angle β. Thus $S = S(H, R, \phi, \beta)$ and $\epsilon_\lambda = \epsilon_\lambda (H, R, A_\lambda)$, where $H = (h/r_o)$ and $R = (r/r_o)$.

Equation (1) can be rearranged into a different form as $\epsilon_\lambda = F - \epsilon_{\lambda c}$, where F is the configuration factor

$$F \equiv \frac{1}{\pi}\int_\beta \int_\phi \sin\beta \cos\beta \, d\beta \, d\phi \qquad (2)$$

and $\epsilon_{\lambda c}$ can be regarded as the contribution due to the finite absorption

coefficient of the gas body

$$\epsilon_{\lambda c} = \frac{1}{\pi} \int_{\beta} \int_{\phi} e^{-A_\lambda S} \sin\beta\cos\beta \, d\beta \, d\phi \tag{3}$$

A more convenient form for the integration of F and $\epsilon_{\lambda c}$ can be accomplished by introducing β', the projection of polar angle β onto the vertical plane as shown in Fig. 1, where $\tan \beta = \sec \phi \tan \beta'$. Thus, the configuration factor can be written as:

$$F = \frac{2}{\pi} \int_{o}^{\beta_o'} \int_{o}^{\phi_o} \frac{\cos^2\phi \, \tan\beta' \sec^2\beta'}{(\cos^2\phi + \tan^2\beta')^2} \, d\beta' \, d\phi \tag{4}$$

where $$\beta_o' = \frac{1}{2} \left[\tan^{-1} \left(\frac{R-1}{H}\right) + \tan^{-1} \left(\frac{R^2-1}{RH}\right) \right] \tag{5}$$

and $\phi_o = \sin^{-1} (1/R)$. Equation (4) can be integrated directly by first integrating with respect to $\tan^2\beta'$ instead of β', and the result is

$$F(H,R) = \frac{1}{\pi} \sin \beta_o' \tan^{-1} (\sin \beta_o' \tan \phi_o) \tag{6}$$

The upper limit β_o' as illustrated in Fig. 1 is being approximated as the arithmetic mean of the two limiting angles, β_1' and β_2', for the partially viewed region due to shielding. In the limiting case of $\beta_o' = \pi/2$ (corresponding to H = 0), an exact result is obtained for Eq. (6) with no shielding, $F(0,R) = (1/\pi) \sin^{-1} (1/R)$.

The term $\epsilon_{\lambda c}$ defined in Eq. (3) can be expressed from simple geometric considerations as:

$$\epsilon_{\lambda c}(H,R) = \frac{2}{\pi} \int_{o}^{\beta_o'} \int_{o}^{\phi_o} e^{-A_\lambda S} \frac{\cos^2\phi \, \tan\beta' \, \sec^2\beta'}{(\cos^2\phi + \tan^2\beta')^2} \, d\beta' \, d\phi \tag{7}$$

where the dimensionless path length as shown in Fig. 1 is given by

$$S(R,\beta',\phi) = \frac{2}{\tan^2\beta'} \left(1-R^2 \sin^2\phi\right)^{1/2} \left(\cos^2\phi + \tan^2\beta'\right)^{1/2} \qquad (8)$$

The integral in Eq. (7) must be evaluated numerically at different locations specified by H and R. Two asymptotic expressions for $\epsilon_{\lambda c}$, however, can be obtained through direct integration. In the case of no shielding (H = 0), the asymptotic expression of ϵ_λ for $A_\lambda \ll 1$ is given as:[2]

$$\epsilon_\lambda(0,R) = \frac{4A_\lambda}{\pi} \left[R\, E_2\left(\frac{\pi}{2}, \frac{1}{R}\right) - \left(\frac{R^2-1}{H}\right) E_1\left(\frac{\pi}{2}, \frac{1}{R}\right) \right] \qquad (9)$$

where E_1 and E_2 are the elliptic integrals of the first and second kinds, respectively. For large R, the spectral apparent emissivity can be expressed as $\epsilon_\lambda(0,R) = A_\lambda/R$. For the case with shielding ($H \neq 0$), the result for $A_\lambda \ll 1$ and $R \gg 1$ can be derived as:[2]

$$\epsilon_\lambda(H,R) = \frac{A_\lambda}{R} \sin\beta_o' \qquad (10)$$

Numerical results for the spectral apparent emissivity in the base plane of a semi-infinite cylindrical gas body are presented in Fig. 2. They were obtained by use of a 7090 Digital Computer. In comparison with the numerical results, the asymptotic expression is found to be a good approximation for $A_\lambda < 0.1$. It should be noted that all the above results are directly applicable to the calculation of the total apparent emissivity if the gray-gas assumption is employed. In that case, $A_\lambda = A$, and $\epsilon_\lambda = \epsilon$.

The total apparent emissivity can be calculated without making the gray

gas assumption by utilizing the concept of mean path length. In view of the expression in Eq. (1), a dimensionless mean path length L may be conveniently defined as

$$\epsilon_\lambda \equiv F\ (1-e^{-A_\lambda L}) \tag{11}$$

When $A_\lambda \ll 1$, $\epsilon_\lambda \approx FA_\lambda L$, which can be compared with the asymptotic expression of ϵ_λ for H = O and $A_\lambda \ll 1$, and gives

$$L(O,R) = \frac{4}{\sin^{-1}(1/R)} \left[RE_2\ (\tfrac{\pi}{2},\ \tfrac{1}{R}\ ) - (\tfrac{R^2-1}{R}\ )\ E_1\ (\tfrac{\pi}{2}\ ,\ \tfrac{1}{R}\ ) \right] \tag{12}$$

A numerical check reveals that the values of ϵ_λ obtained by use of the mean path length, Eq. (11) and Eq. (12), agree very well with the numerically calculated results for all values of A_λ. It is also obvious that the agreement becomes exact at two limits, A_λ = O and $A_\lambda \to \infty$. This indicates that the restriction of $A_\lambda \ll 1$ can also be removed, although no rigorous proof has been established here.

For the case with shielding (H ≠ O) a semi-empirical equation is suggested as

$$L(H,R) = \frac{4 \sin \beta_o'}{\tan^{-1} (\sin\beta_o' \tan \phi_o} \left[RE_2\ (\tfrac{\pi}{2},\ \tfrac{1}{R}\ ) - (\tfrac{R^2-1}{R})\ E_1(\tfrac{\pi}{2},\tfrac{1}{R}) + \frac{\pi \cos^2 \beta_o'}{16\ R^3} \right] \tag{13}$$

The above equation is chosen based on the consideration that it should reduce to Eq. (12) as H → O, and to the asymptotic expression of L for $A_\lambda \ll 1$, $R \gg 1$, based on Eq. (10). Again, the comparison between the values of ϵ_λ

obtained from Eqs. (11) and (13), and the numerical results from the computer indicates that the condition $A_\lambda \ll 1$ is not necessary in the present case. The values of L as a function of H and R are plotted in Fig. 3. With the expression of L as given in Eq. (13), one can calculate the total apparent emissivity with a given infrared absorption spectrum according to

$$\epsilon(H,R) = F \sum_i (1-e^{-A_i L}) \ (D_{2i}-D_{1i}) \tag{14}$$

where the functions

$$D_{ni}(\lambda_{ni},T) \ \frac{1}{\sigma T^4} \int_o^{\lambda_{ni}} \frac{\pi \, c_1 \, d\lambda}{\lambda^5 \ [\exp(c_2/\lambda T)-1]} \tag{15}$$

are called the relative cumulative spectral radiance of a black body, and are tabulated as a function of temperature and frequency.[3] The constants c_1 and c_2 are the radiation constants in the Planck distribution.

By using the available absorption measurements for CO_2 and H_2O at high temperatures[4,5] numerical calculations have been performed and the results are presented in Figs. 4 and 5.* For CO_2 at 2500 ^oR and 1 atm., it is found by comparing Fig. 4 with corresponding ϵ_λ-figures, Fig. 2, that the effective wavelength-independent coefficient A is about 0.05 for all four values of H. For H_2O at 2000 ^oR and 1 atm., the value of A is about 0.25 for different values of H.

---

* A more exact numerical calculation based on the line-of-sight integration has been reported by S. deSoto (S. deSoto, The Radiation From an Axisymmetric, Real Gas System With a Non-Isothermal Temperature Distribution, presented at the Seventh National Heat Transfer Conference, Cleveland, Ohio, August, 1964). As shown in Figs. 6 and 7, the approximate results of this report are in good agreement with the more accurate calculations.

A procedure for calculating the apparent emissivity of conical gray-gas bodies has been given in ref. 2. Numerical results were obtained for conical gas bodies of apex angles of 20, 60 and 120 degrees.

Calculations of Mean Path Length for a Radiating Gas

It has been demonstrated in the previous section that the use of mean-path-length concept greatly simplifies the analysis of the probe. The numerical calculation of the final results, however, still relies on a given infrared spectrum. The scope of this calculation technique would be increased if the formulation of mean path length is based on certain general relations about infrared absorption instead of the detailed knowledge of infrared spectrum. Recently, Olfe[6] has studied the mean path length based on various theoretical band absorption models, and has obtained expressions of the mean path length for some simple enclosure geometries. However, in view of the recent experimental evidence, a more realistic calculation[7] of mean path length is feasibly by use of the experimentally established expressions for band absorptivity[8,9]. Indeed, these expressions could also be supported by certain theoretical arguments[8,10].

The radiant energy flux, based on a single band, from an isothermal gas volume to a differential element of its confining surface is given by

$$H = \frac{1}{\pi} \int_{\Omega} \int_{\omega} \int_{\rho} R_{\omega} \cos \phi \, \frac{d \, \epsilon_{\omega} (\rho)}{d \, \rho} \, d\rho \, d\omega \, d\Omega \equiv R_{\omega} \, A(L) \tag{16}$$

and

$$A(\rho) = \int_{\omega} \epsilon_{\omega} (\rho) \, d\omega \tag{17}$$

where the identity in equation (16) defines the mean path length L. In equation (16), Ω is the solid angle subtended by a gas volume, ω the wave number, ρ the distance between the differential element on the confining surface and the differential gas volume, R_ω the Planck function for monochromatic blackbody radiant energy, ϕ the angle between ρ and the normal to the differential element, $\epsilon_\omega(\rho)$ the spectral emissivity for a gas of path length ρ, $\bar{R}_\omega$ the average value of R_ω in the wave-number interval of the emission band, and A the band emissivity. Under the approximation $R_\omega \approx \bar{R}_\omega$ in the emission wave-number interval, equation (16) becomes

$$A(L) = \frac{1}{\pi} \int_\Omega A(r) \cos \phi \, d\Omega \tag{18}$$

where the integration with respect to ρ in equation (16) is carried out from zero to r. In the limiting case of transparent gas, the spectral emissivity and consequently the band emissivity will be directly proportional to r and there follows from equation (18)

$$L^o = \frac{1}{\pi} \int_\Omega r \cos \phi \, d\Omega \tag{19}$$

which is the mean path length for a transparent gas.

It should be noted that with the approximations $R_\omega(T_g) \approx \bar{R}_\omega(T_g)$ and $R_\omega(T_s) \approx \bar{R}_\omega(T_s)$ in a single band, where T_g and T_s denote temperatures of gas and source respectively, the band emissivity A is identical to the band absorptivity. In the following, the mean path length will be calculated based on two experimentally established correlations for the band absorptivity,

A(r).

Recent experimental studies [8,9] have indicated that the power-law type of correlation

$$A = C\, w^{a}\, P_e^{\,b} \quad (0.5 \le a \le 1,\ 0 \le b \le 0.5) \tag{20}$$

applies successfully to a substantial region of the mass path length w (the product of geometric path length r and the partial pressure of the absorbing gas, and the equivalent pressure P_e (a pressure which takes account of differences between self-broadening and foreign-gas broadening[11]). This correlation includes as its special cases the well known relations $A \propto W$ for non-overlapping weak lines and $A \propto (w\, P_e)^{0.5}$ for non-overlapping strong lines. But it further suggests that there exists a substantial range of w and P_e in which non-overlapping strong lines and weak lines appear together in the band . Substitution of equation (20) into (18) results in

$$L = \left[\frac{1}{\pi} \int_{\Omega} r^{a} \cos \phi \, d\Omega \right] \tag{21}$$

In writing equation (21) it has been assumed that all the path lengths r of the gas enclosure are in the range such that equation (20) holds. However, extension to gas enclosures consisting of various ranges of absorption correlation poses no particular problem.

For a spherical enclosure, $r = D \cos \phi$ where D is the diameter of the sphere, equations (19) and (21) give

$$\frac{L}{L^{o}} = \frac{3}{2} \left(\frac{2}{2+a} \right)^{1/a}, \quad L^{o} = \frac{2}{3} D \tag{22}$$

For an enclosure consisting of two infinite parallel planes, $r = h/\cos\phi$ where h is the thickness of the plane layer, there follows

$$\frac{L}{L^o} = (1/2)\left(\frac{2}{2-a}\right)^{1/a}, \quad L^o = 2h \tag{23}$$

The result for an infinite circular cylindrical enclosure of diameter D is

$$\frac{L}{L^o} = \left[\frac{\left(\frac{2+a}{2}\right) \quad \left(\frac{3-a}{2}\right)}{\left(\frac{3+a}{2}\right) \quad \left(\frac{4-a}{2}\right)}\right], \quad L^o = D \tag{24}$$

For a finite cylindrical enclosure, the path length to the center of the base is $r = R/\sin\phi$ for $\phi \geq \phi_o$ and $r = h/\cos\phi \leq \phi_o$, where R is the radius of the cylinder, h the height and $\phi_o = \tan^{-1}(R/h)$. The mean path length to the center of the base can be found as

$$\frac{L}{L^o} = \frac{1}{L^o}\left[\left(\frac{2\,h^a}{2-a}\right)(1-\cos^{(2-a)}\phi_o) + \left(\frac{2\,R^a}{2-a}\right)(1-\sin^{(2-a)}\phi_o)\right] \tag{25}$$

and $$L^o = 2\left[h(1-\cos\phi_o) + R\,(1-\sin\phi_o)\right] \tag{26}$$

In the previous treatment of mean path length by Olfe[6], the band width $\Delta\omega$ is taken as a fixed constant value. This is approximately correct as long as the band does not become saturated. When a portion of the band becomes saturated, the band wing will spread out. Consequently, instead of approaching an upper limit, the band absorptivity will increase continuously with the increasing mass path length and equivalent pressure. The correlation of logarithmic form[8,9]

$$A = E + F \ln (w P_e^m) \quad (m \leq 1) \tag{27}$$

has been found to represent successfully this spread effect at very large values of w and P_e. From equations (18) and (27), the mean path length for the present case is expressed as

$$L = \exp\left[\frac{1}{\pi}\int_{\Omega} (\ln r)\cos\phi \, d\Omega\right] \tag{28}$$

where the assumption has also been made that all the path lengths of the gas enclosure are in the range such that equation (27) holds. The expression of mean path length for various simple geometries are

$$\frac{L}{L^o} = \frac{3}{2} e^{-1/2} = 0.910 \tag{29}$$

for a spherical enclosure

$$\frac{L}{L^o} = (1/2)e^{1/2} = 0.825 \tag{30}$$

for an enclosure consisting of two infinite parallel planes,

$$\frac{L}{L^o} = 4e^{-3/2} = 0.892 \tag{31}$$

for an infinite circular cylindrical enclosure, and

$$\frac{L}{L_o} = \frac{1}{L_o}\exp\left[(\ln h)\sin^2\phi_o + (\ln R)\cos^2\phi_o + (\ln \sin\phi_o)\sin^2\phi_o + (\ln \cos\phi_o)\cos^2\phi_o + 1/2\right] \tag{32}$$

for radiation to the center of the base of a finite circular cylinder.

The above discussion of mean path length based on the power-law and

logarithmic expressions of band absorptivity could be easily extended to the calculation of radiation from a cylindrical gas body to its outer base.

For the specific enclosure geometries considered above, it can be readily seen that in the whole range from small to very strong absorption, $L < L^o$. This criterion can be shown to hold for all enclosure geometries. From Equations (19), (21) and (28), it follows

$$\int_\Omega \left(\frac{r}{L^o} - 1\right) \cos\phi \, d\Omega = \int_\Omega \frac{1}{a}\left[\left(\frac{r}{L_p}\right)^a - 1\right] \cos\phi \, d\Omega = \int_\Omega \left(\ln \frac{r}{L_1}\right) \cos\phi \, d\Omega = o$$

where L_p and L_1 denote the mean path length based on the power-law and the logarithmic absorption correlations, respectively. Since for $0.5 \leq a \leq 1$

$$\left(\frac{r}{L} - 1\right) \geq \frac{1}{a}\left[\left(\frac{r}{L}\right)^a - 1\right] \geq \ln \frac{r}{L}$$

the following inequality must hold

$$L^o \geq L_p \geq L_1$$

Therefore, the mean path length L^o is the upper limit of the mean path length L based on the experimentally established absorption correlations.

For the case that the geometric beam length r is independent of solid angle Ω (i.e., a hemisphere) equations (19), (21) and (28) give $L^o = L_p = L_1$. In other words, for enclosure geometries having relatively small variation of r, $L^o \approx L_p \approx L_1$. This is also confirmed in the results for the specific enclosure geometries considered.

EXPERIMENTAL DETERMINATION OF INFRARED ABSORPTION OF HIGH-TEMPERATURE GASES

Introduction

Theoretical determination of the infrared spectra of high-temperature gases is often formidable due to the increasing complexity of the excited states at high temperatures[12]. Consequently, many experimental systems have been developed recently for infrared measurements of gases at high temperatures. They can be classified into three groups: (1) combustion systems[13, 14], (2) shock tubes[15,16] and furnaces[17,18,19]. The different gases which can be studied with a combustion system (open exhaust jet) are limited. Moreover, because of band interference of various species, it may not be possible to determine the infrared absorption due to the particular species under investigation. The shock-tube system probably provides the most accurate results for spectral absorption, but due to the extremely short time for observation, only one measurement at a specific wavelength can be made during one test. Thus the shock-tube system is impractical for detection of the entire infrared spectrum of a gas. In both combustion and shock-type systems, it is also very difficult to vary the thermodynamic and optical conditions of the gas, such as the temperature, pressure and path-length. With furnace systems, absorption measurements of a variety of gases can be made and a more flexible control of thermodynamic and optical conditions is possible. Such apparatus

has been limited to the temperatures up to about 1200 ^{o}K, however, because of optical window and other material limitations.

In the present work, the design of a new furnace system, which will operate at temperatures up to about 2000 ^{o}K is described. The apparatus consists essentially of a graphite resistance furnace with an inner ceramic tube for containment of high-temperature gases, and an optical system for detection of infrared absorption. Data on the CO fundamental band have been obtained at temperatures of 300 ^{o}K and 1800 ^{o}K for path-lengths of 10 cm and 20 cm and pressures varying from (1/4) to 3 atmospheres. Comparison with existing experimental data[15,20] shows agreement within 15 percent.

Infrared Absorption Systems

The apparatus for infrared spectral absorption studies is shown schematically in Fig. 8. A photograph of the system in the laboratory is presented in Fig. 9. It consists of: (1) a globar source with a chopper blade for alternating the input to the energy sensing element, (2) a high temperature furnace which incorporates the gas test cell, (3) a monochrometer and (4) an amplifier and automatic recorder.

High Temperature Furnace

The details of the high temperature furnace* are shown in Fig. 10. The test gas is contained in a zirconia tube. This is surrounded by a cylindrical

---

* Manufactured by the Astro Corporation, Santa Barbara, California.

graphite heater. Because of the oxidation of graphite at high temperatures, a system is provided for maintaining an inert gas atmosphere around the heating element. This region is sealed from the test cell which is supplied from an independent gas system.

The electrodies and the outer surface of the furnace are water cooled. A radial tube opening to the bottom makes it possible to measure the temperatures of the zirconia tube or graphite heater with an optical pyrometer.

The test optical path is limited to the central isothermal zone of the furnace by use of water-cooled window holders at each end. The windows are made of hot-pressed zinc selenide* which is transparent in the 1 - 20 μ wavelength region. This material is inert to H_2O, CO_2, and CO in the temperature range below 550 ^{o}K. The design of these water-cooled window holders allows for adjustment of the test path-length. As shown in Fig. 10, the test gas is supplied to the zirconia tube through passages within the window probes. Two connections are provided on each probe, but at present only one on each side is used. This allows one connection to be used for flushing and pressure control.

The radiative and conductive heat fluxes to the ends of the probes are very large, especially at higher temperatures. This heat flux must be reduced in order to minimize the radial temperature distribution through the zirconia tube. Preliminary tests indicated that excessive temperature differences across the tube can cause the failure of the zirconia tube. A

---

* Eastman Kodak Irtran 4.

molybdenum-discilicide coated molybdenum radiation shield is used to reduce the flux to the window probes. This shield is 1.5 inches in diameter, 0.030 inch thick, and 3.0 inches long. The inner end is closed with a disc spot-welded to the tube shield. The test beam passes through a 0.50 inch diameter hole in the center of the disc.

Gas Supply System

A flow diagram of the gas supply system is shown in Fig. 11. Commercial gas cylinders (CO or CO_2) are connected to the two small stainless steel micro-regulating valves for adjusting the test gas pressure inside the zirconia tube. After the stainless steel micro-regulating valves there is a compound pressure gauge located in the line leading to the furnace through the window probes.

The water vapor supply system consists of a steam generation unit and accompanying control valves. The purpose of the steam generation unit is to provide high-purity steam for absorption measurements and to reduce corrosion of components in the furnace. It consists of a stainless steel water storage tank pressurized with inert gas, a water preheater, and a stainless steel deaerator to eliminate dissolved gases. A regulating valve is located in the line connecting the deaerator and the evaporator for adjusting the amount of water going to the evaporator. The supply line is wrapped with heating wire to eliminate the possibility of vapor condensing between the evaporator and the furnace.

The inert gas supply consists of pressurized N_2, He, or Ar bottles and a two-way pressure regulator. In the line from the regulator and the furnace

there is a compound pressure gauge. The inert gas not only supplies the furnace, but is used to regulate the pressure in the steam generation unit, and also for flushing the optical system.

Furnace Exhaust

The furnace exhaust system is designed to provide proper pressure control for the absorbing and inert atmospheres and for flushing. Control of the pressure in the furnace is accomplished by the two stainless steel micro-regulating valves and the two-way pressure regulator mentioned earlier. The test gas exhaust and the inert exhaust are connected to a vacuum pump via a surge tank. A reciprocating piston vacuum pump is used at present, but for future work with water vapor, a water-driven ejector pump has been provided. The vacuum obtained with either system is 29.5 inches Hg; the maximum pressure recommended in the furnace is 35 psig.

Optical System

Figure 1 shows the main components of the optical system; the source, absorption cell, and the detection assembly. The source assembly directs chopped collimated infrared radiation through the absorption cell (gas containment system) into the detector, which measures the relative spectral distribution of the transmitted radiant energy.

The energy is supplied to the optical system by a high-temperature globar which can be electrically heated to about 1100 ^{o}C. The globar used is a silicon carbide rod 3/16 inch in diameter, and two inches long. The

beam is focused by a spherical mirror on a chopper-rectifier unit which differentiates the energy of the source (globar) from the energy radiated by the gas. The aluminum chopper blade is blackened on the side facing the absorption cell to eliminate reflection of energy emitted by the gas. All mirrors in the optical system have aluminum surfaces because of their high reflectivity in the infrared region. The chopped energy is collimated by an off-axis paraboloid mirror and directed through the gas containment system by a plane mirror, as shown in Fig. 8. The source components are contained in an 11 inch by 7 inch by 28 inch steel box. This container is evacuated and then filled with inert gas (N_2 or argon).

The partially absorbed beam, combined with the emitted energy from the gas, is then focused by an off-axis paraboloid mirror in the entrance slit of a double-pass monochromator (Perkin-Elmer Model 99). The Model 99 double-pass monochromator makes use of part of the same optical system twice to provide monochromatic radiation of high spectral resolution.

The beam from the monochrometor prism is focused on a thermocouple detector maintained in a vacuum. The A.C. component of the thermocouple output resulting from the transmitted energy of the source is amplified by a preamplifier in the monochromator and by the Model 107 amplifier, and then recorded by a Leeds and Northrop Speedomax recording potentiometer. The wavelength drive unit used consists of a variable speed D.C. motor connected to a reduction gear box. The mirror box and the monochromator are connected to the inert gas supply so that they can be purged with dry gas when in operation.

Gas Temperature Distribution

One of the objectives of the present study is to determine the effect of temperature on the absorption of radiant energy by gases. For this reason it is desirable that the temperature along the absorption path-length be as uniform as possible. To investigate the temperature distribution in the test zone a thermocouple probe was designed and mounted in one of the water-cooled window holders (see Fig. 12). This probe was fabricated from 1/16 inch O.D. platinum sheathed cable containing platinum-platinum 13% rhodium wires in magnesium oxide. The thermocouple junction was surrounded by two concentric platinum radiation shields, 1/4 inch and 1/2 inch in diameter, respectively. The probe was positioned axially by means of a traversing screw thread. Typical temperature measurements are shown in Fig. 13. It is apparent from Fig. 13 that at temperatures above 1200 ^{o}K the temperature of the gas along the optical path-length is not uniform. Variations are of the order of 300 ^{o}K. A rough estimate of this effect shows that the actual path-length may deviate from the equivalent isothermal path-length by 15 percent or less. There are several possible furnace modifications to improve this temperature non-uniformity, such as by controlling the axial resistance of the graphite heater, and by employing ceramic winder holders to withstand high temperatures. Data reported in the following section, however, were obtained without such system modifications.

Results for Carbon Monoxide

Initial testing has been conducted with CO at temperatures of 300 ^{o}K and 1800 ^{o}K for path-lengths of 10 cm and 20 cm and pressures from (1/4) to 3 atmospheres. In order to account for optical effects outside of the absorption path-length, a reference run is made for each test condition. The optical resolution of the monochromator being used is not high enough to detect line shapes (i.e., the optical slit-width is larger than the line half-width). Because of this, Lambert-Beer's law can not, in general, be used for the analysis of experimental data. Therefore, to avoid any a priori assumption of band structure to analyze the data, it is necessary that there be no residue-gas absorption during the reference run (accomplished by purging with a non-absorbing gas). Under these conditions

$$T_a' = T_t \, T_r' \tag{33}$$

where T_t is the spectral transmissivity of the test gas, T' is a measured quantity proportional to transmissivity and the subscripts a and r denote absorption and reference runs respectively. Equation (33) holds regardless of the band structure as long as the transmissivities for reference runs are nearly grey. Care must also be taken to select a slit-width which will not affect the measurements of spectral absorptivity over the range of wave-lengths being investigated.

Room Temperature Results

Carbon monoxide at room temperature conditions has been extensively studied[12,20]. A set of measurements of CO at the room temperature (300 ^{o}K) was therefore made to check with these existing data. Figures 14 and 15 show two sets of spectral absorptivities at path-lengths of 10 cm and 20 cm respectively for pressures of 1/4, 1/2, 1, 2 and 3 atmospheres. The integrated band absorptivities A,

$$A = \int \alpha_{\omega} \, d\omega \qquad (34)$$

Table 1: Integrated Band Absorptivies in Cm^{-1} of CO Fundamental at 300 ^{o}K

	path length = 10 cm		path length = 20 cm	
Pressure in atm	Present	Burch and Williams[20]	Present	Burch and Williams[20]
1/4	45	42	66	60
1/2	89	85	122	110
1	148	120	169	150
2	184	160	210	190
3	205	185	226	210

The present results are consistently higher than Burch and Williams results (data by Penner and Weber[12] is not in the present range), but the deviation

is less than 10 percent. This considered to be acceptable for this type of measurement.

High Temperature Results

Shown in Figs. 16 and 17 are two sets of spectral absorptivities at 1800 ^{o}K for path-lengths of 10 cm and 20 cm, respectively, and pressures of 1, 1-1/2, 2, 2-1/2 and 3 atmospheres. The only existing results which can be compared with the present study are those of Davies' shock-tube study[15]. He obtained spectral absorptivities of CO at wavelengths of 4.60, 4.67 and 4.72 μ for temperatures from 1160 ^{o}K to 2300 ^{o}K. Since data are given at different temperatures and path-lengths from those of present data, a linear relation was used for the interpolation of temperatures and the Lambert-Beer's law was used for the interpolation of path-lengths. These interpolations are, of course, approximate. The comparison of present results averaging over different pressures based on data at a path-length of 10 cm with those of Davies is shown in the following table:

Table 2: Spectral Intensities in atm^{-1} cm^{-1} of CO Fundamental at Temperature of 1800 ^{o}K

	4.60 μ	4.67 μ	4.72 μ
Present	0.053	0.040	0.046
Davies[15]	0.054	0.035	0.035

The agreement is very good considering the different experimental conditions and the approximate interpolations used in the comparison.

According to the theory of molecular spectroscopy, the intensities of fundamental bands are temperature-independent, while the intensities of non-fundamental bands (overtone, combination and difference bands) are temperature-dependent. And the variation in the intensities can be satisfactorily described by a harmonic-oscillator approximation. Therefore, the ratio of relative magnitudes of intensities of non-fundamental bands to those of fundamental band increases with temperature. At high temperature, this yields , insteady of a simple fundamental band at room temperature, a composite band composed of non-fundamental bands as well as simple fundamental band in the 2143 cm^{-1} region. The composite band can be adequately described by random Elsasser model or are statistical model, which is the limiting case of the random Elsasser model when the number of components, N, of the random Elsasser model increases.

The main characteristic of the statistical model for lines with a Lorentz shape can be expressed by the formula[18]

$$T_w = \exp \left[- \left(\frac{w}{d}\right) P \right] \qquad (35)$$

where T_w is the spectral transmissivity, P the pressure, d the average line spacing, w the average equivalent width at unit pressure. The quantity (w/d) is a function of temperature and path-length but not a function of pressure. The data given in Figs. 16 and 17 are calculated to show whether the values of (w/d) can be correlated according to the statistical model. The results are shown in Figs. 18 and 19 for the path-lengths of 10 cm and

20 cm respectively. The data points in Fig. 17 show relatively fair agreement while those in Fig. 19 do not correlate so well.

Weak-Line Approximation

In the weak-line approximation region Lambert-Beer's law is valid. Hence for the same optical path-length (product of pressure and geometrical path-length) absorptivities are expected to be equal. A check on this point will easily reveal whether the gaseous conditions are in this region for a certain band. This is done in Figs. 20 and 21 for temperatures of 300 ^{o}K and 1800 ^{o}K respectively. Two experimental curves are shown in Fig. 20 for path-lengths of 10 cm and 20 cm together with the theoretical weak-line approximation curve of Malkmus and Thomson[21] all at room temperature and at an optical path-length of 10 atm-cm. A similar plot of curves at a temperature of 1800 ^{o}K and at an optical path-length of 30 atm-cm is given in Fig. 21. These results indicate that for temperatures at and lower than 1800 ^{o}K and for path-lengths at and larger than 10 cm the weak-line approximation does not hold. With further decrease of the path-length, the weak-line approximation will eventually be satisfied. Further increase of temperature may also cause an approach to weak-line approximation, because as the line population becomes higher and higher, lines smear out and become continuous.

REFERENCES

1. E.R.G. Eckert and R.M. Drake, Jr., Heat and Mass Transfer, p. 388, McGraw-Hill Book Co., Inc., New York (1959).

2. C.L. Tien and M.M. Abu-Romia, "Radiative Energy Transfer to the Outer Base Regions of Cylindrical and Conical Gas Bodies", Institute of Engineering Research Report No. AS-63-4, University of California, Berkeley, California (1963).

3. N. Pivonsky, Tables of Blackbody Radiation Functions, The MacMillan Co., New York (1961).

4. D.K. Edwards, J. Opt. Soc. A., 50, 130 (1960).

5. K.E. Nelson, "Experimental Determination of the Band Absorptivities of Water Vapor at Elevated Pressures and Temperatures," M.S. Thesis, Univ. of Calif., Berkeley, Calif. (1959).

6. D.B. Olfe, JQSRT, 1, 169-176 (1961).

7. R.V. Dunkle, Trans. ASME J. Heat Transfer, C 86, 75-61 (1964).

8. J.N. Howard, D. E. Burch and D. Williams, J. Opt. Soc. Amer. 46, 237-245 (1956).

9. D.E. Burch and D. Williams, Appl. Opt. 1, 473-482, 587-594 (1962).

10. D.K. Edwards and W.A. Menard, Appl. Opt. 3, 621-625 (1964).

11. D.E. Burch, E.B. Singleton and D. Williams, Appl. Opt. 1, 359-363 (1962).

12. S.S. Penner, Quantitative Molecular Spectroscopy and Gas Emissivities, Addison-Wesley Co., Reading, Mass. (1959).

13. R.H. Tourin, J. Opt. Soc. Amer. 51, 175 (1961).

14. C.C. Ferriso, J. Chem. Phys. 37, 1955 (1962).

15. W.O. Davies, J. Chem. Phys. 36, 292 (1962).

16. K.G.P. Sulzmann, JQSRT, 4, 375 (1964).

17. J.T. Bevans, R.V. Dunkle, D.K. Edwards, J.T. Gier, L.L. Levenson, and A.K. Oppenheim, J. Opt. Soc. Amer. 50, 130 (1960).

18. U.P. Oppenheim and Y. Ben-Aryeh, J. Opt. Soc. Amer. 53, 344 (1963).

19. R. Goldstein, JQSRT, 4, 343 (1964).

20. D.E. Burch and D. Williams, Appl. Optics, 1 , 587 (1962).

21. W. Malkmus and A. Thomson, JQSRT, 2, 17 (1962).

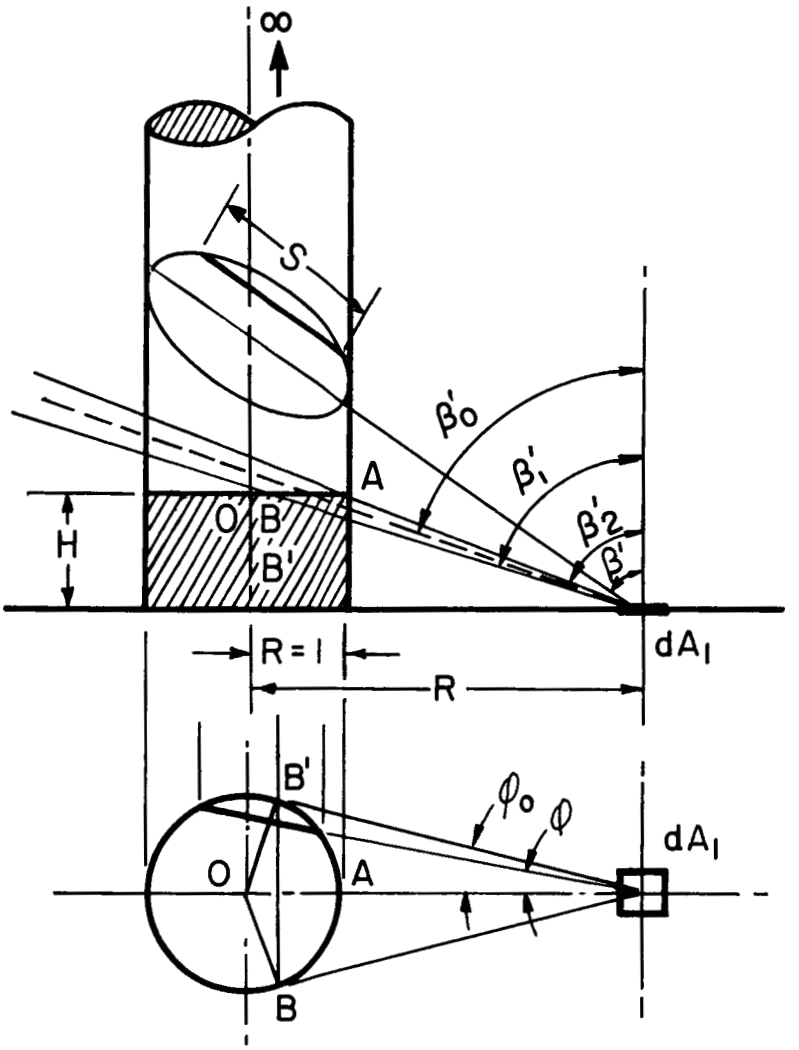

FIG. 1 THE SEMI-INFINITE CYLINDRICAL GAS BODY

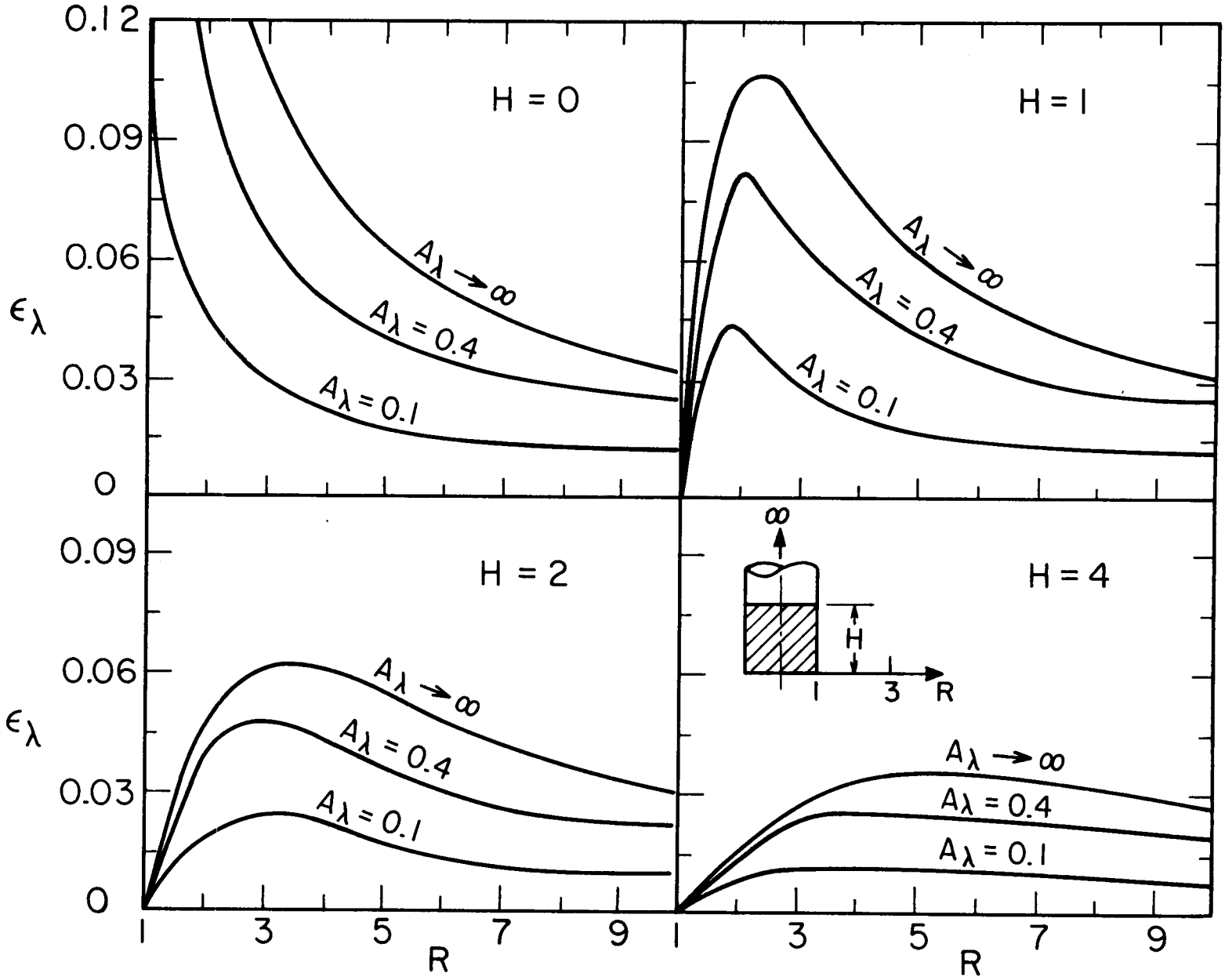

FIG. 2 SPECTRAL APPARENT EMISSIVITY IN THE BASE PLANE OF A CYLINDRICAL GAS BODY

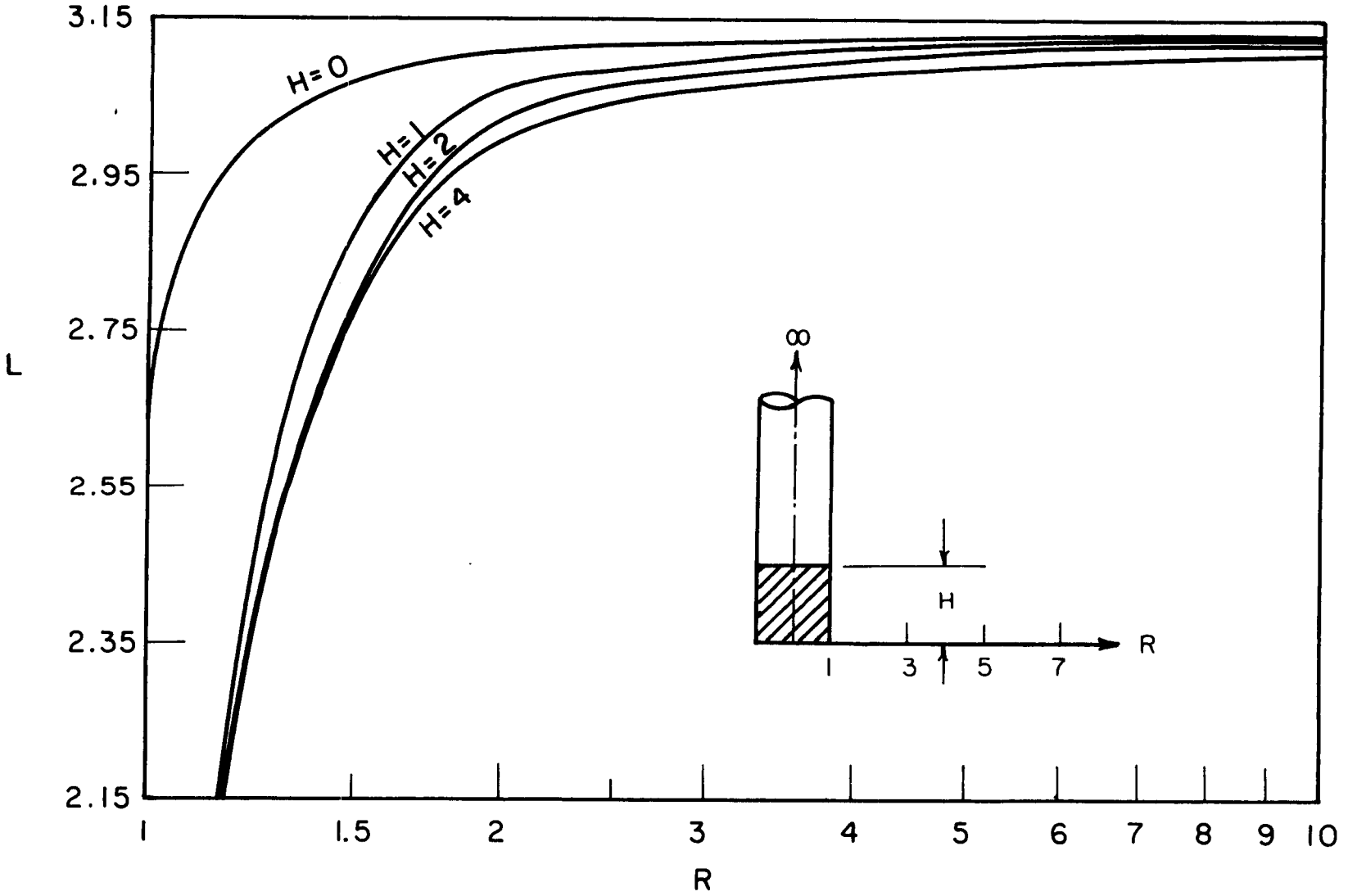

FIG. 3 DIMENSIONLESS MEAN PATH LENGTH FOR THE CYLINDRICAL GAS BODY

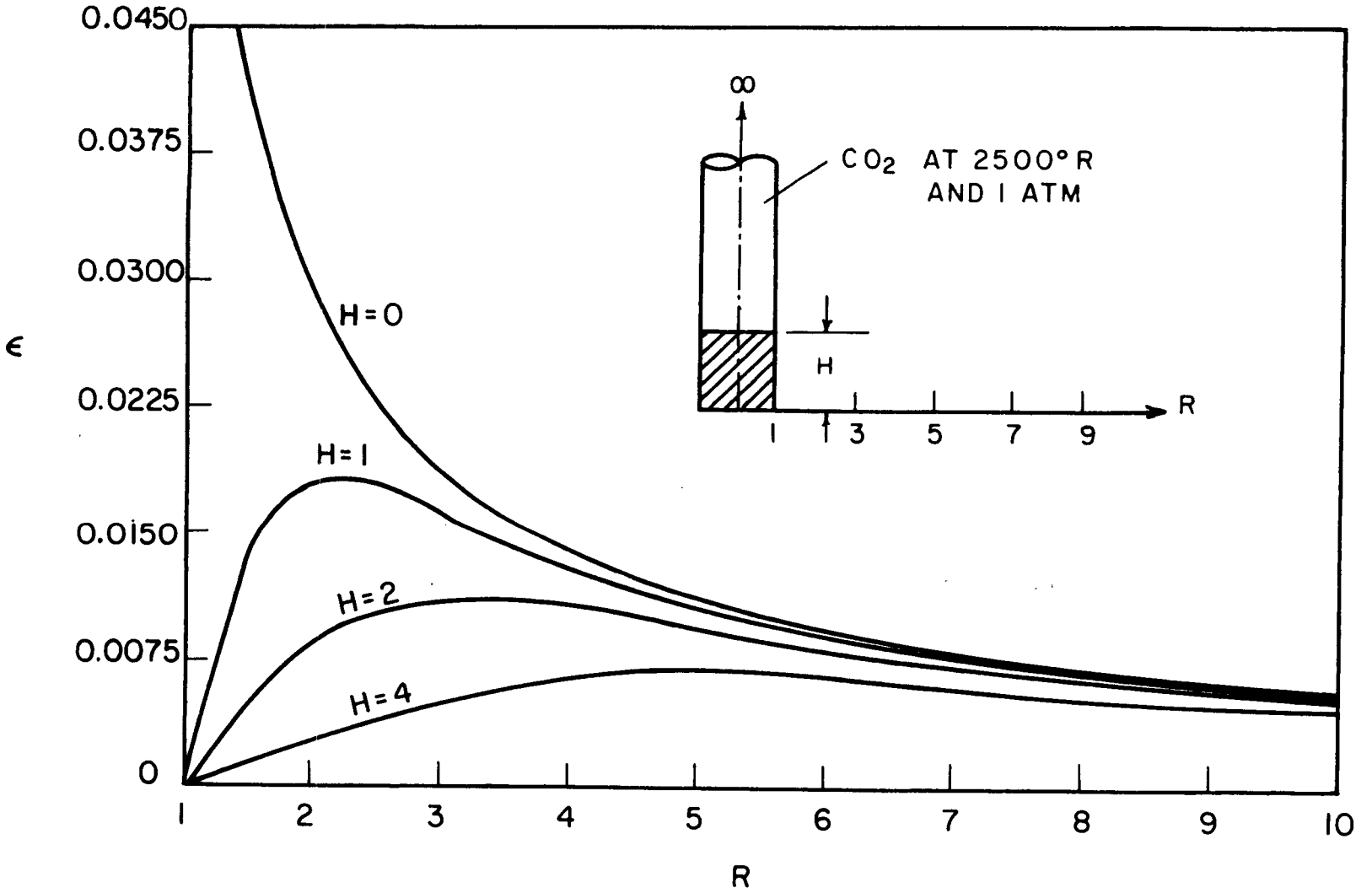

FIG. 4 APPARENT EMISSIVITIES IN THE BASE PLANE OF A SEMI-INFINITE CYLINDER OF CARBON DIOXIDE AT 2500 °R AND ONE ATMOSPHERIC PRESSURE

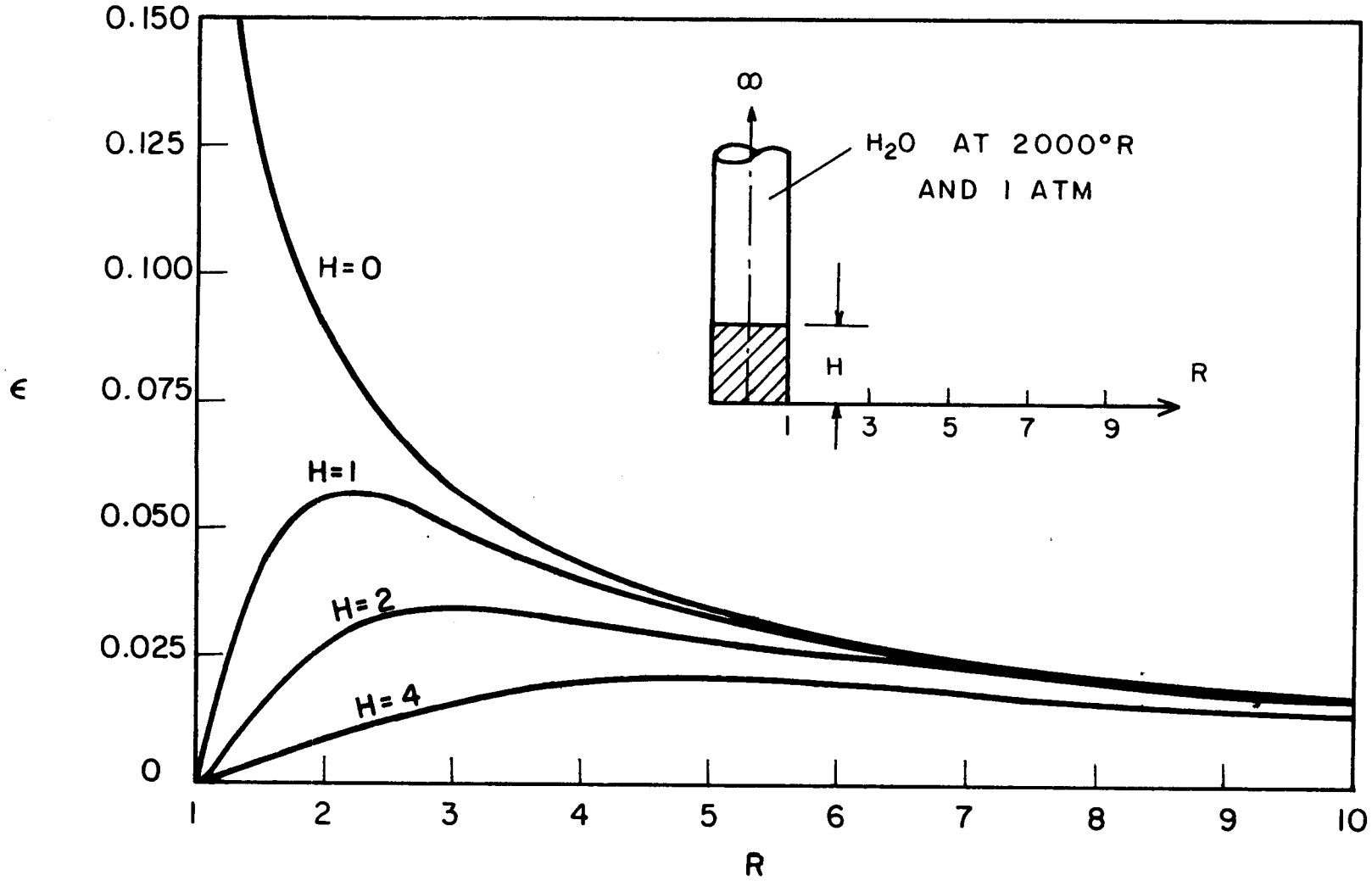

FIG. 5 APPARENT EMISSIVITIES IN THE BASE PLANE OF A SEMI-INFINITE CYLINDER OF WATER VAPOR AT 2000°R AND ONE ATMOSPHERIC PRESSURE

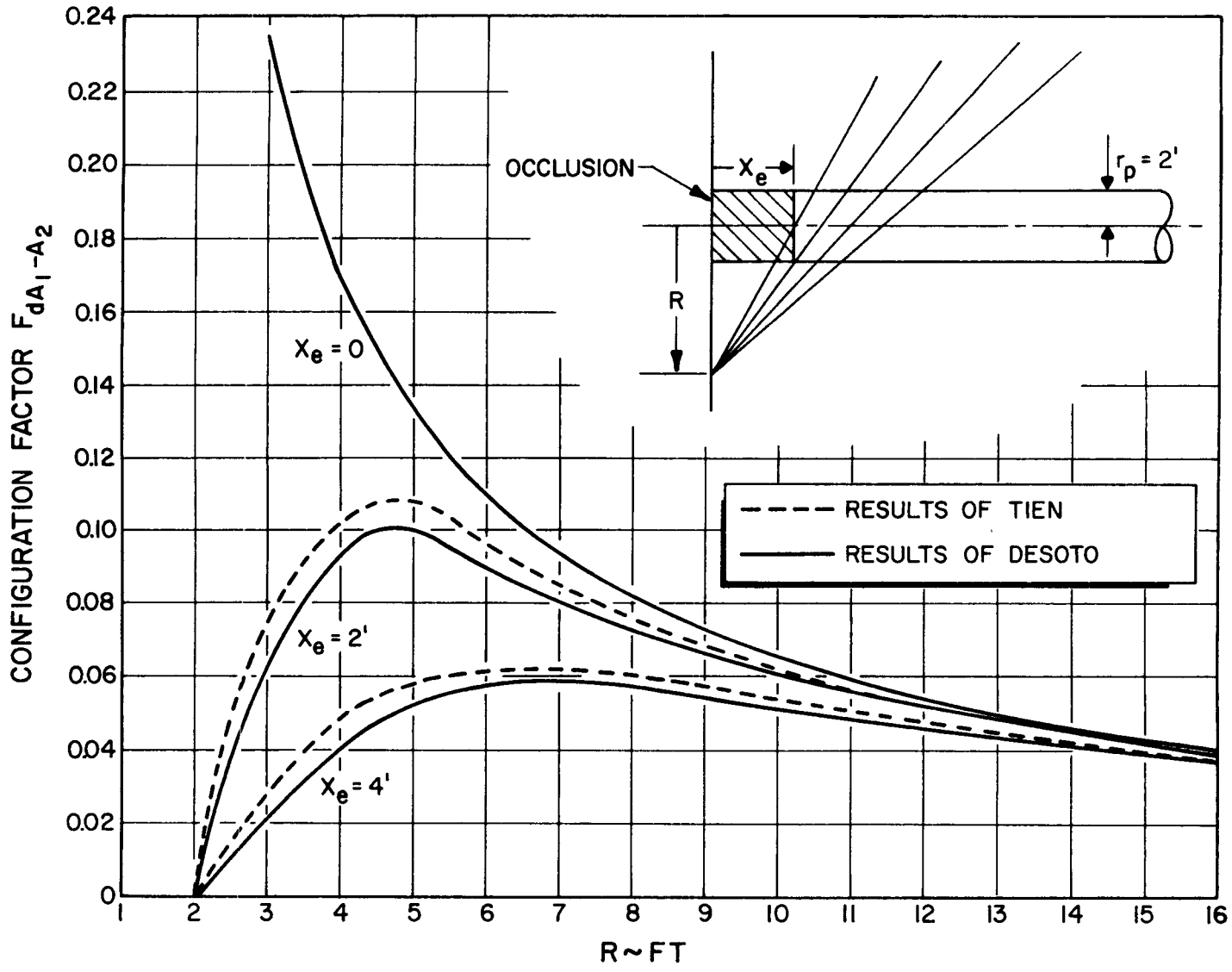

FIG. 6 RADIATION FROM THE CYLINDRICAL GAS TO THE OUTER BASE REGION
(REPRODUCED FROM DESOTO)

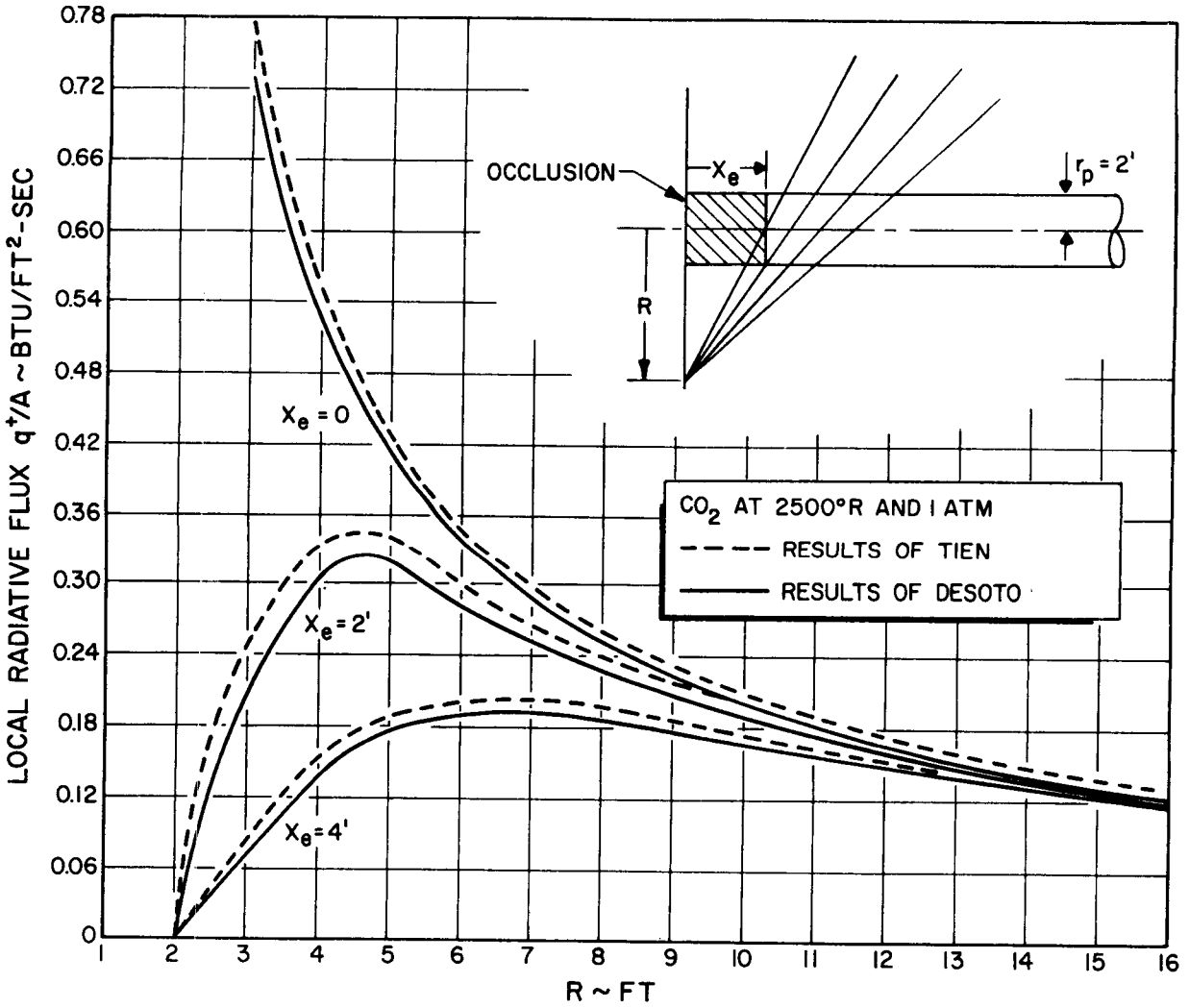

FIG. 7 RADIATION FROM THE CYLINDRICAL GAS TO THE OUTER BASE REGION (REPRODUCED FROM DESOTO)

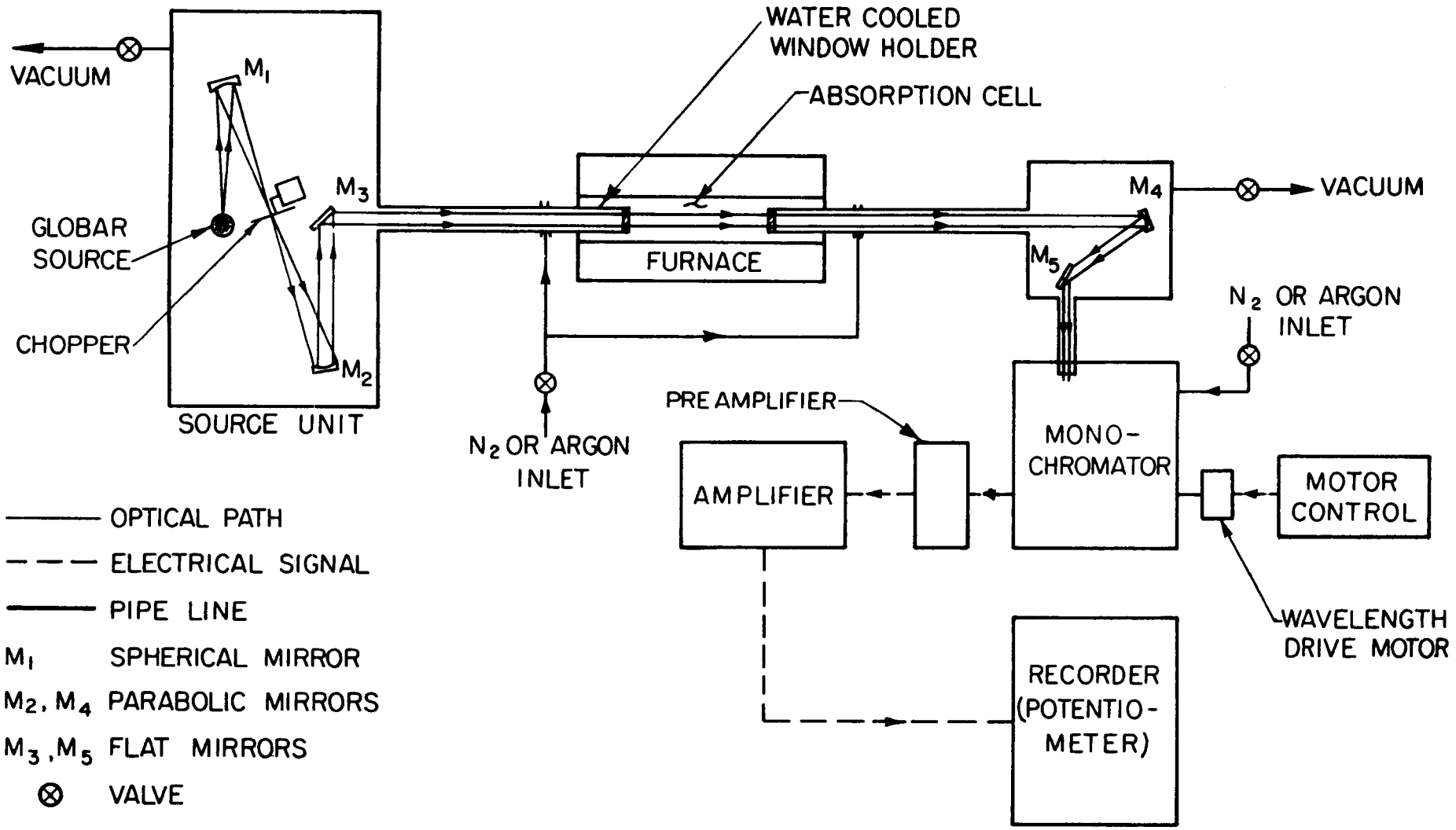

FIG. 8 HIGH TEMPERATURE INFRARED ABSORPTION SYSTEM

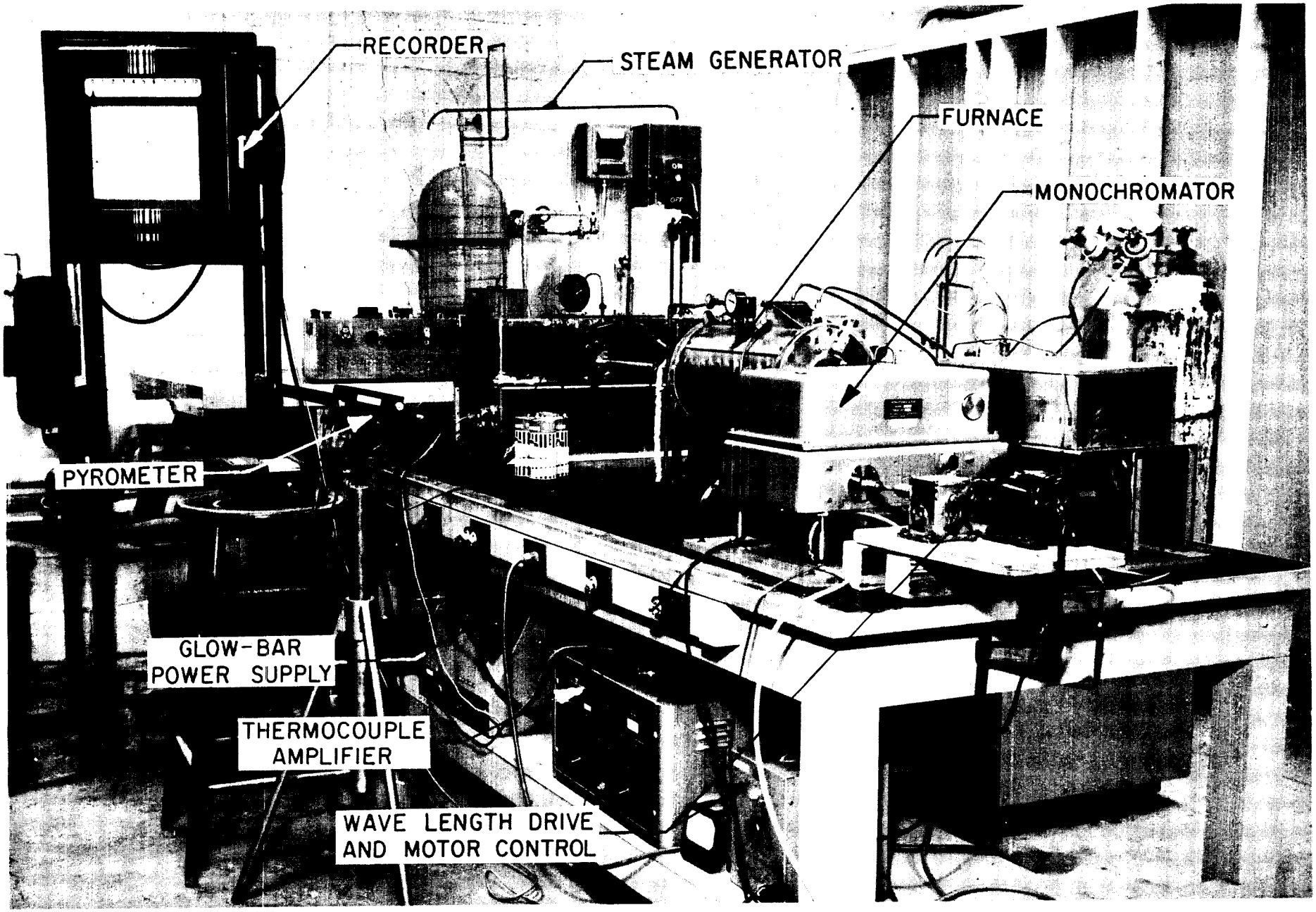

FIG. 9 HIGH TEMPERATURE INFRARED ABSORBTION SYSTEM

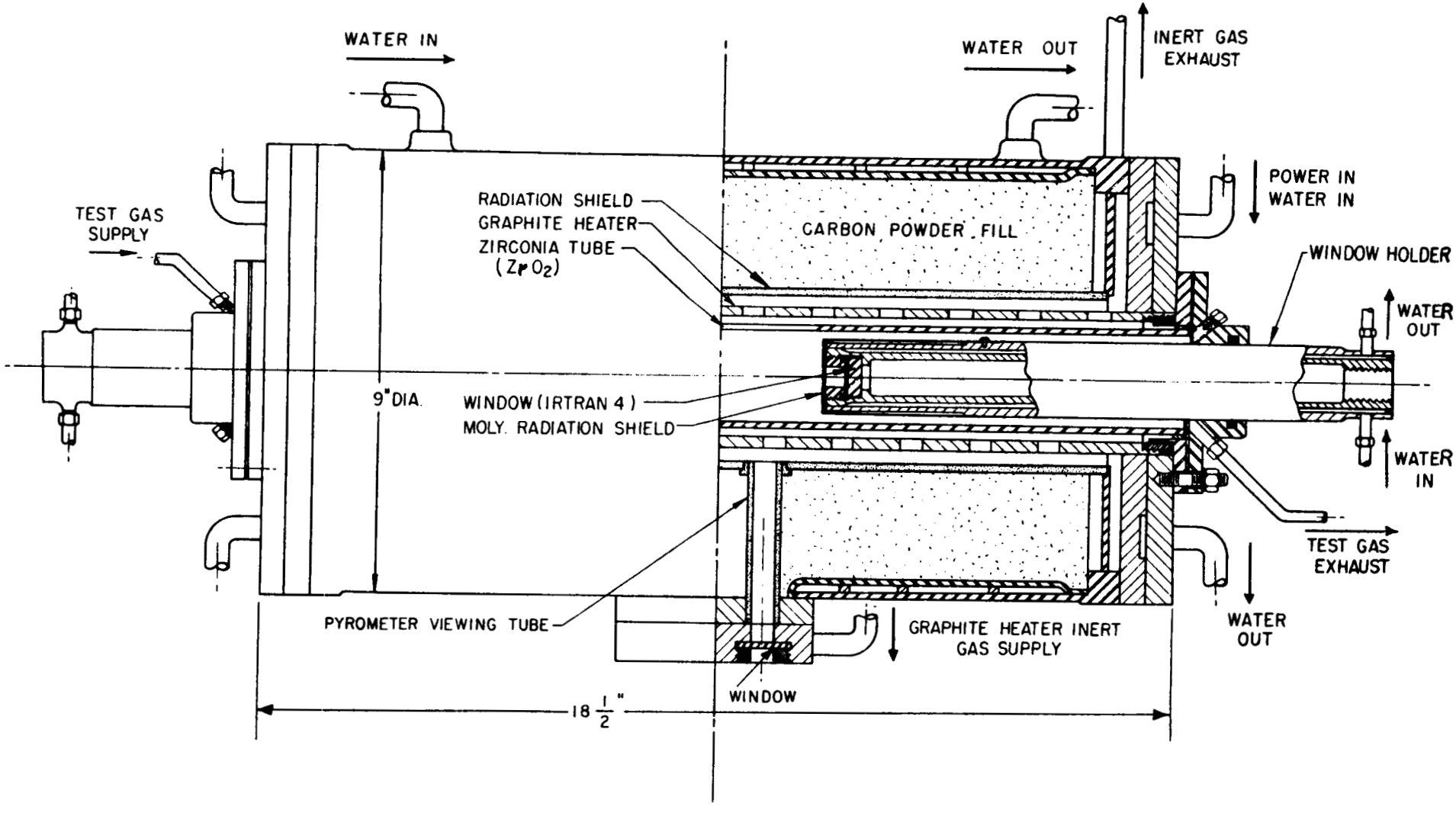

FIG. 10 HIGH TEMPERATURE FURNACE

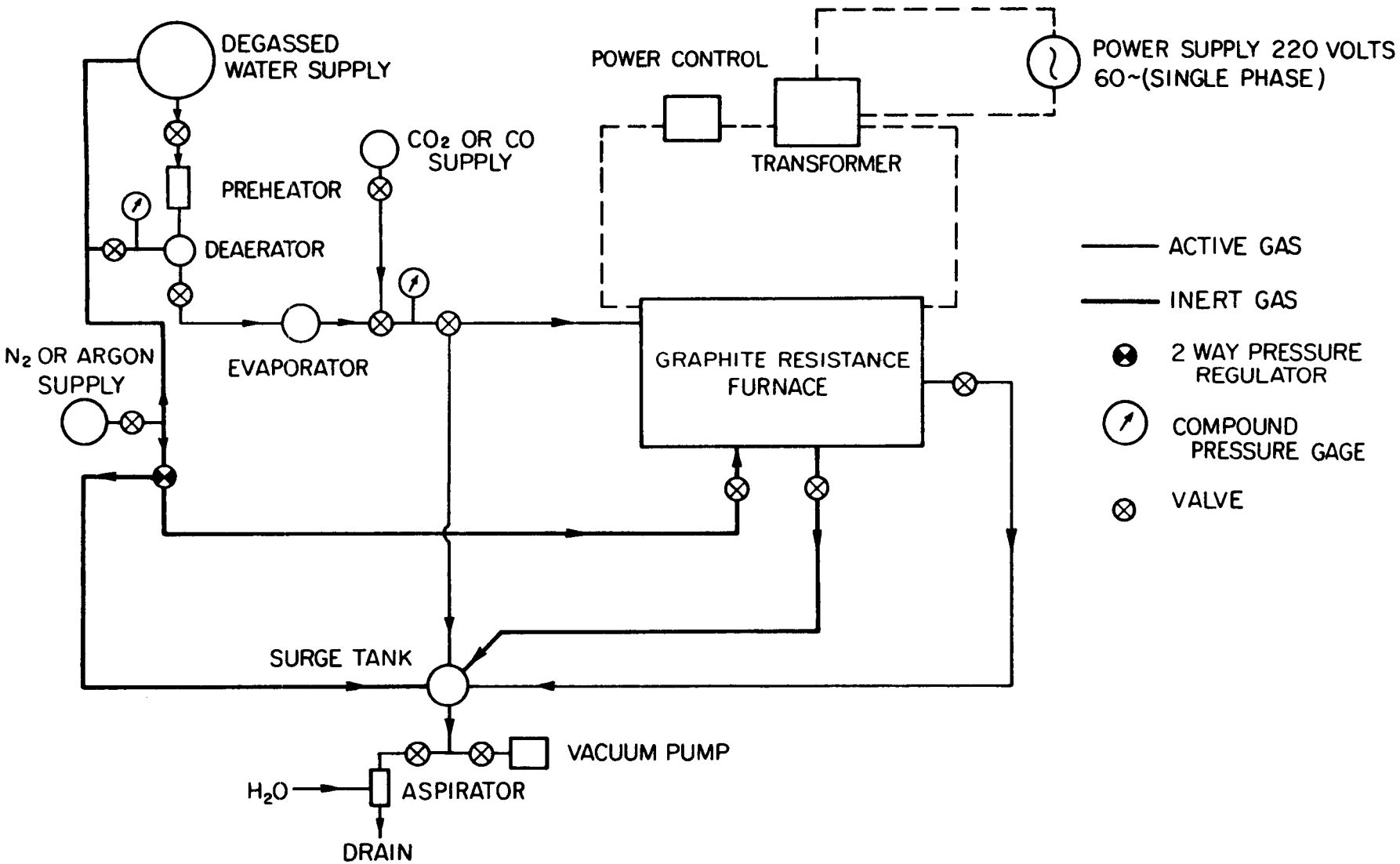

FIG. II GAS SUPPLY SYSTEM

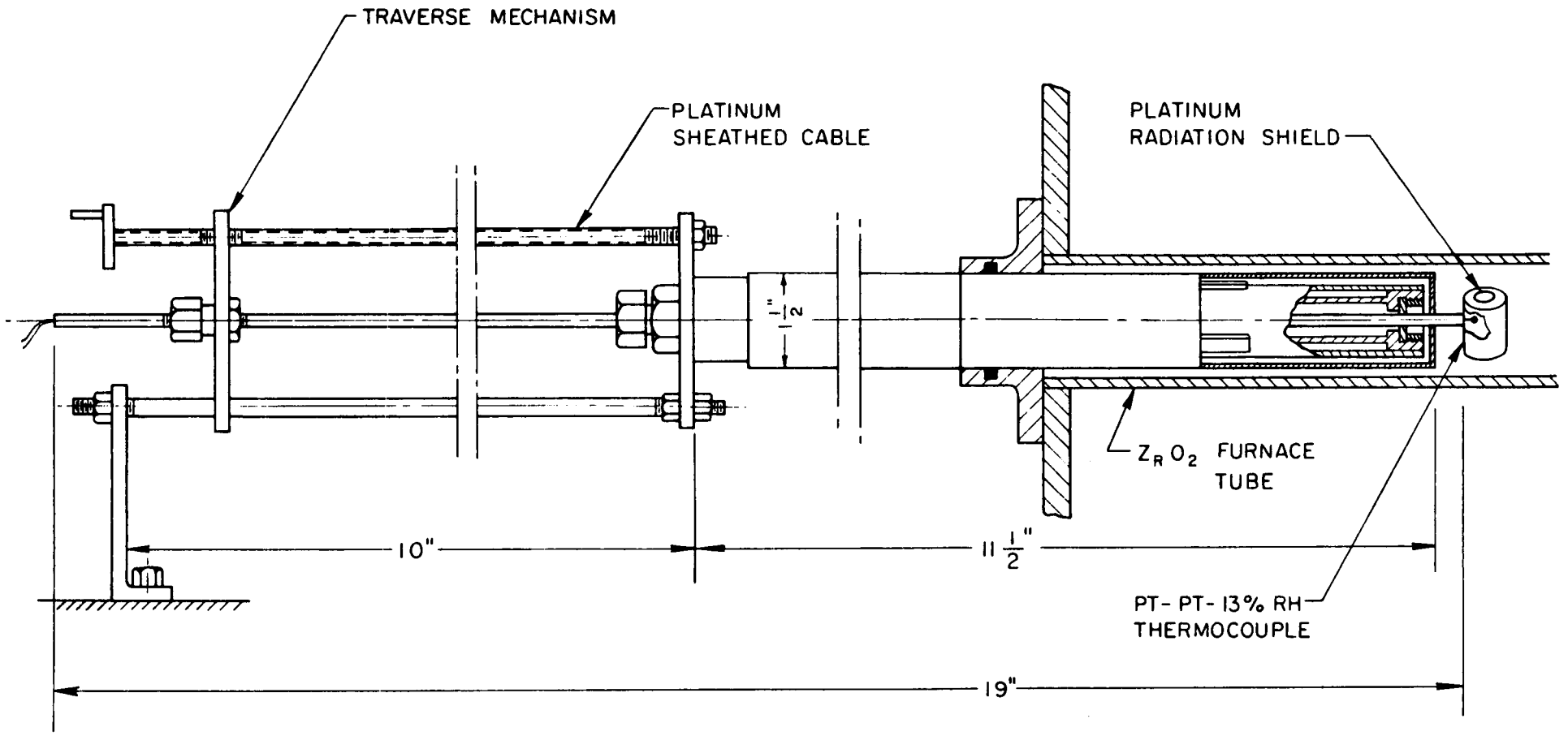

FIG. 12 TEMPERATURE PROBE

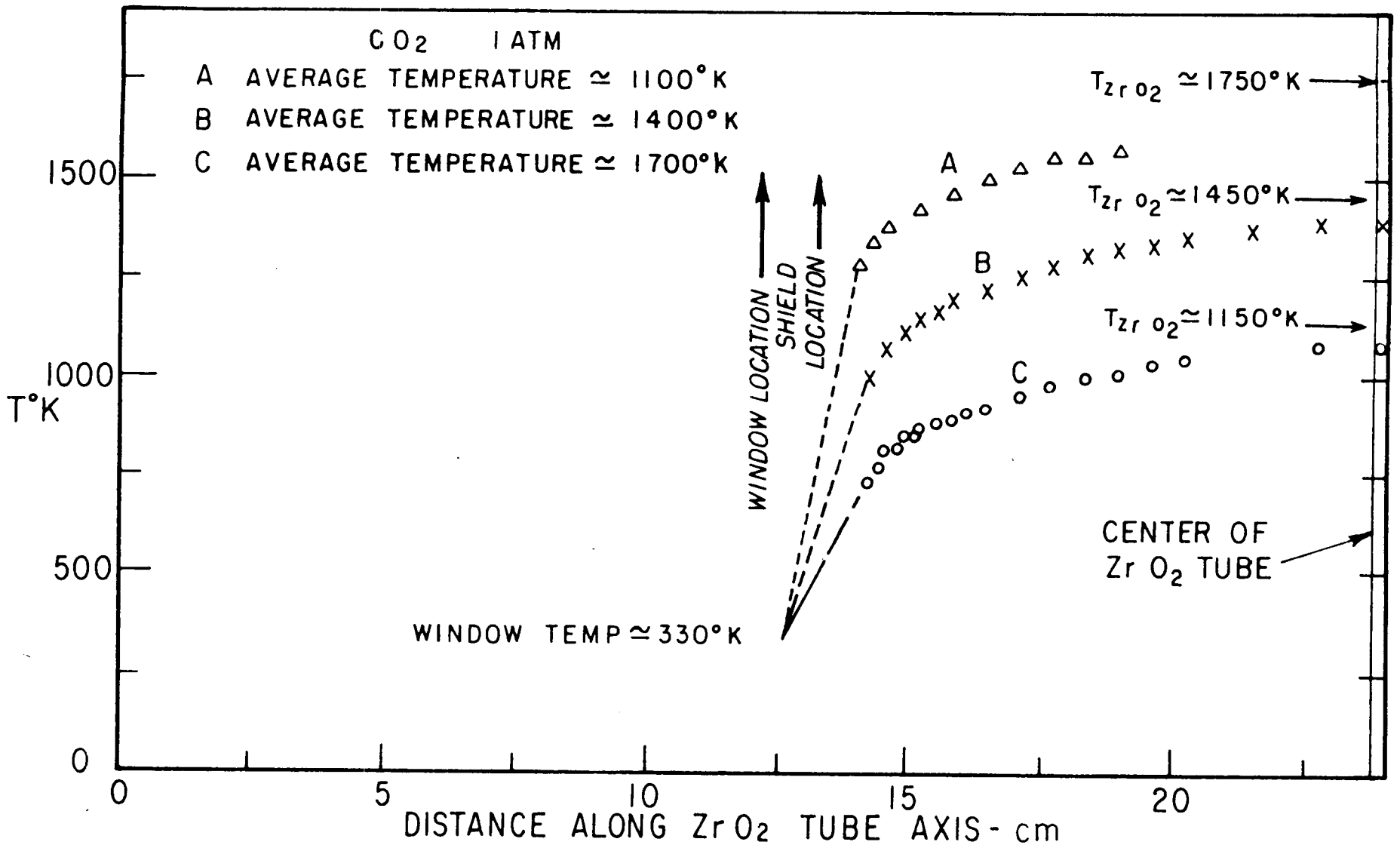

FIG. 13 GAS TEMPERATURE DISTRIBUTIONS

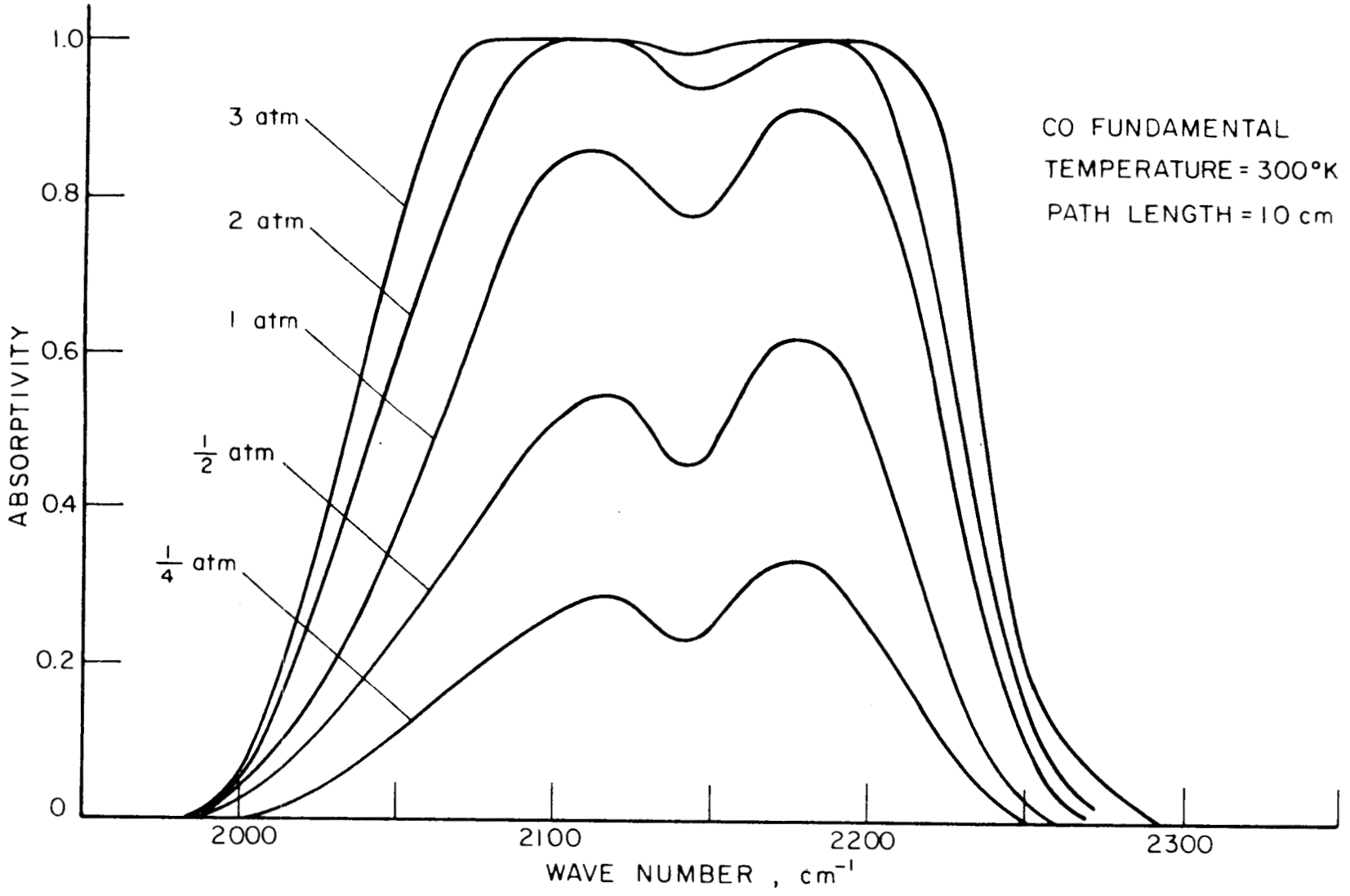

FIG. 14 SPECTRAL ABSORPTIVITY OF CO FUNDAMENTAL AT TEMPERATURE 300 °K AND PATH LENGTH 10 cm

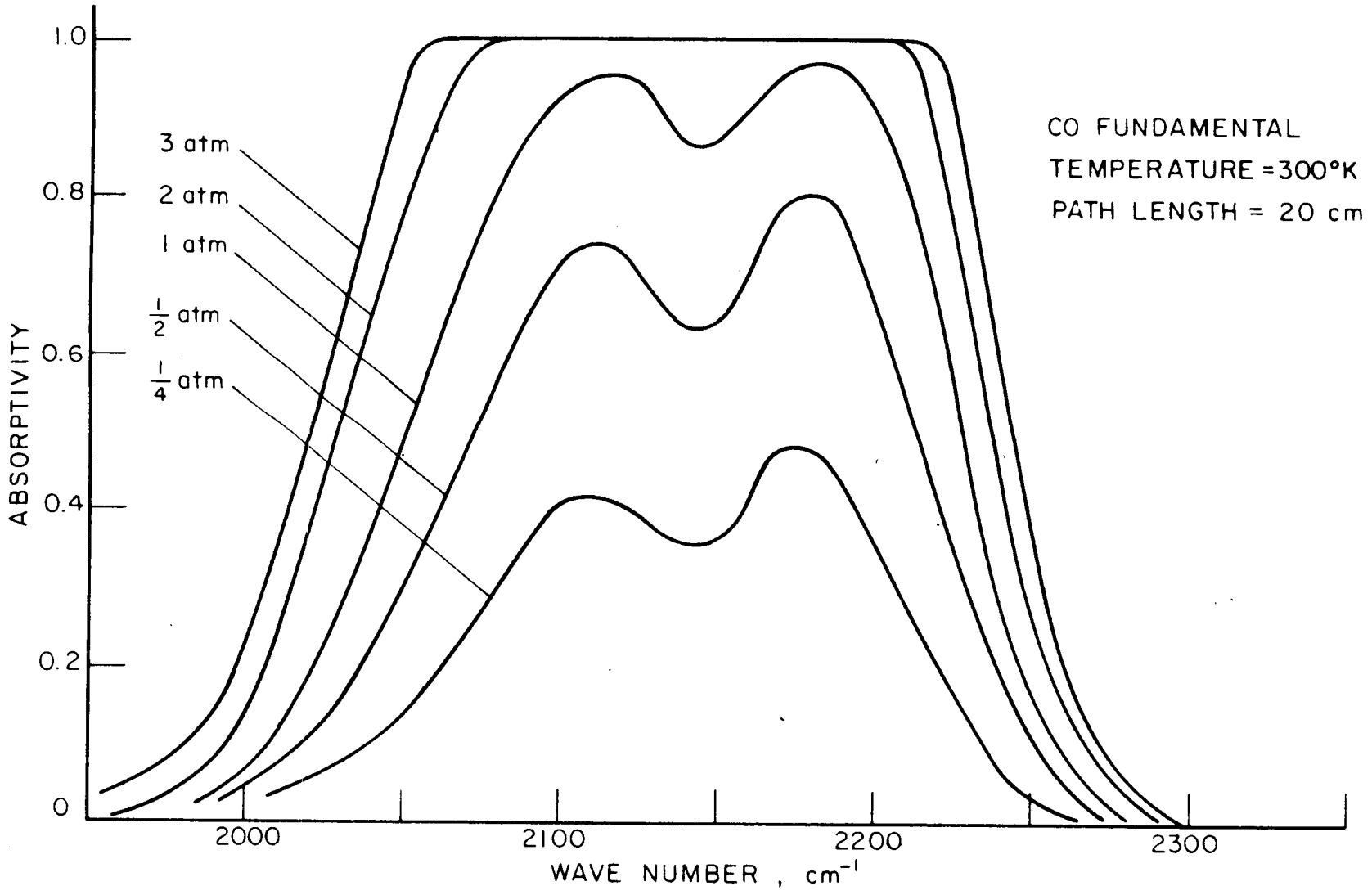

FIG. 15 SPECTRAL ABSORPTIVITY OF CO FUNDAMENTAL AT TEMPERATURE 300 °K AND PATH LENGTH 20 cm

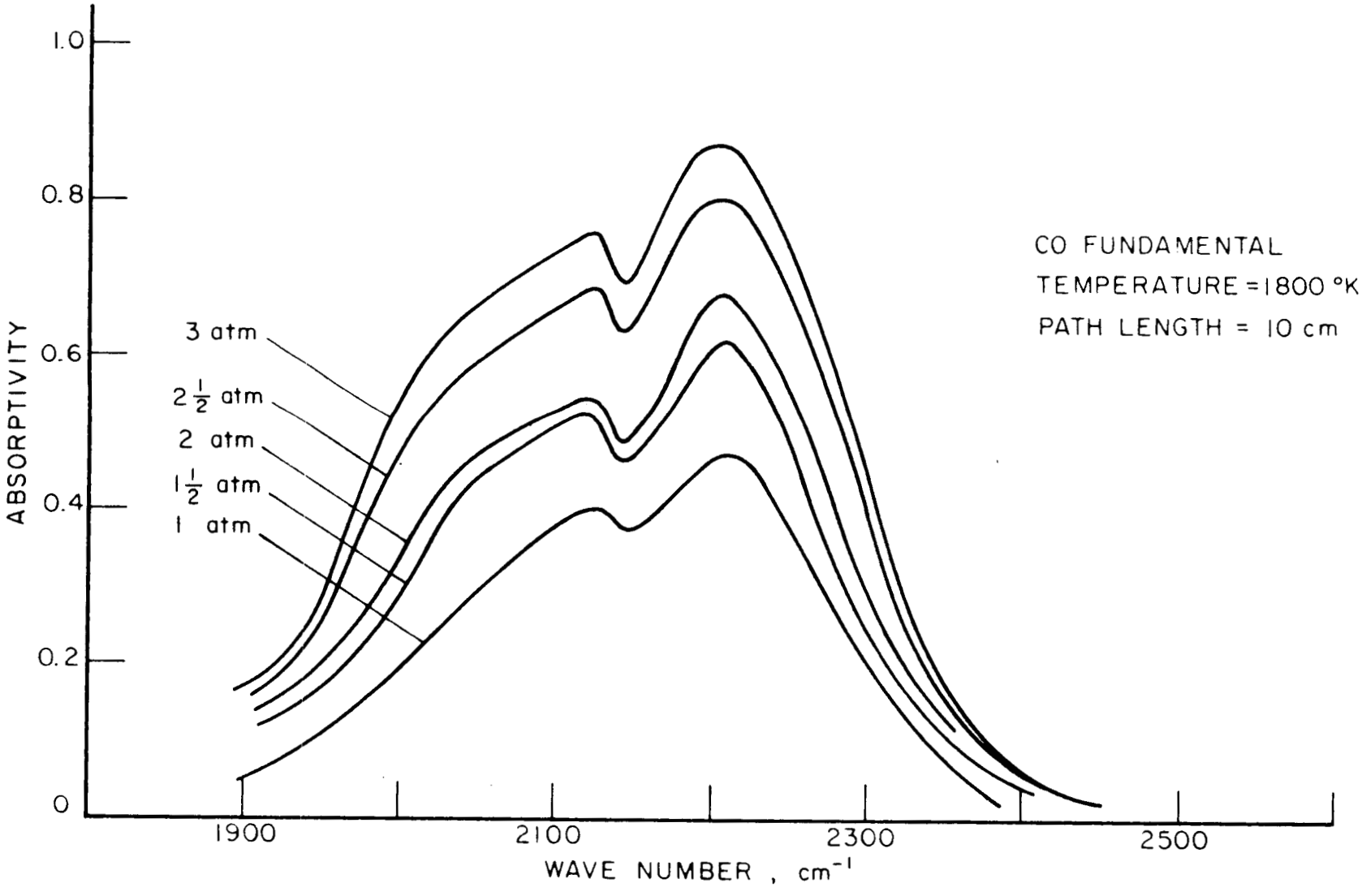

FIG. 16 SPECTRAL ABSORPTIVITY OF CO FUNDAMENTAL AT TEMPERATURE 1800 °K AND PATH LENGTH 10 cm

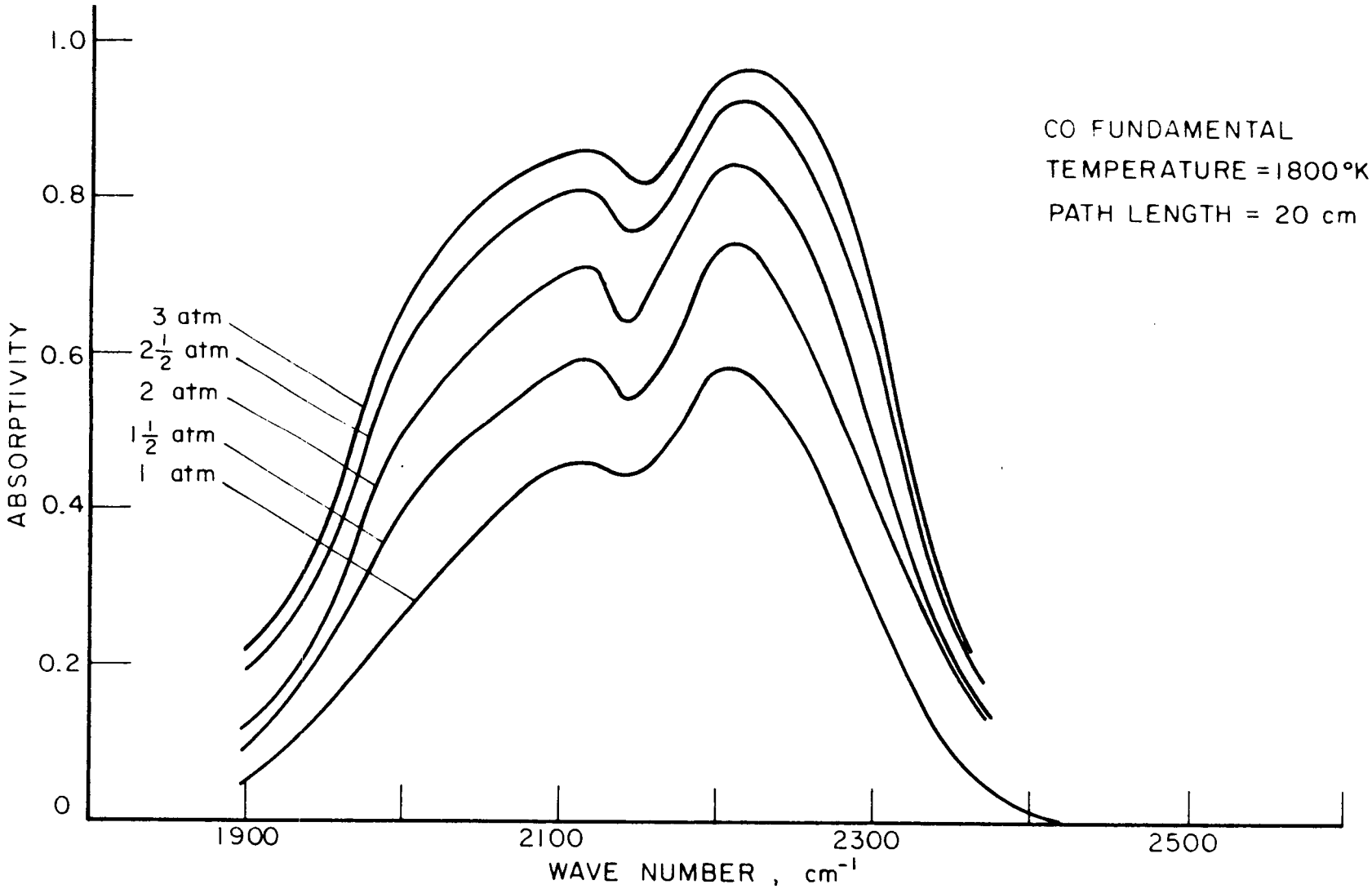

FIG. 17 SPECTRAL ABSORPTIVITY OF CO FUNDAMENTAL AT TEMPERATURE 1800 °K AND PATH LENGTH 20 cm

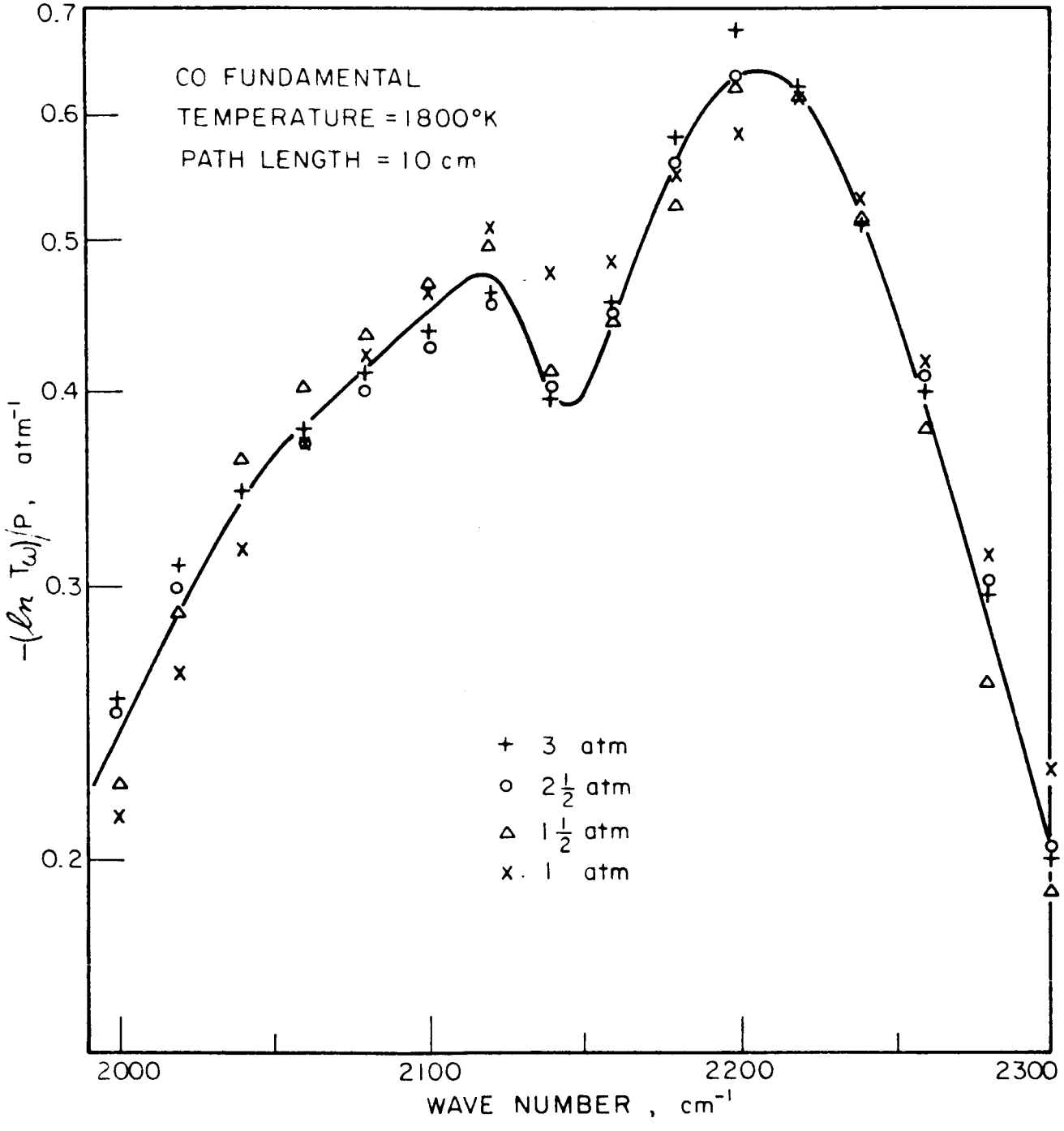

FIG. 18 SPECTRAL VALUES OF $-(\ell n T_\omega)/P$ FOR CO FUNDAMENTAL AT TEMPERATURE 1800°K AND PATH LENGTH 10 cm

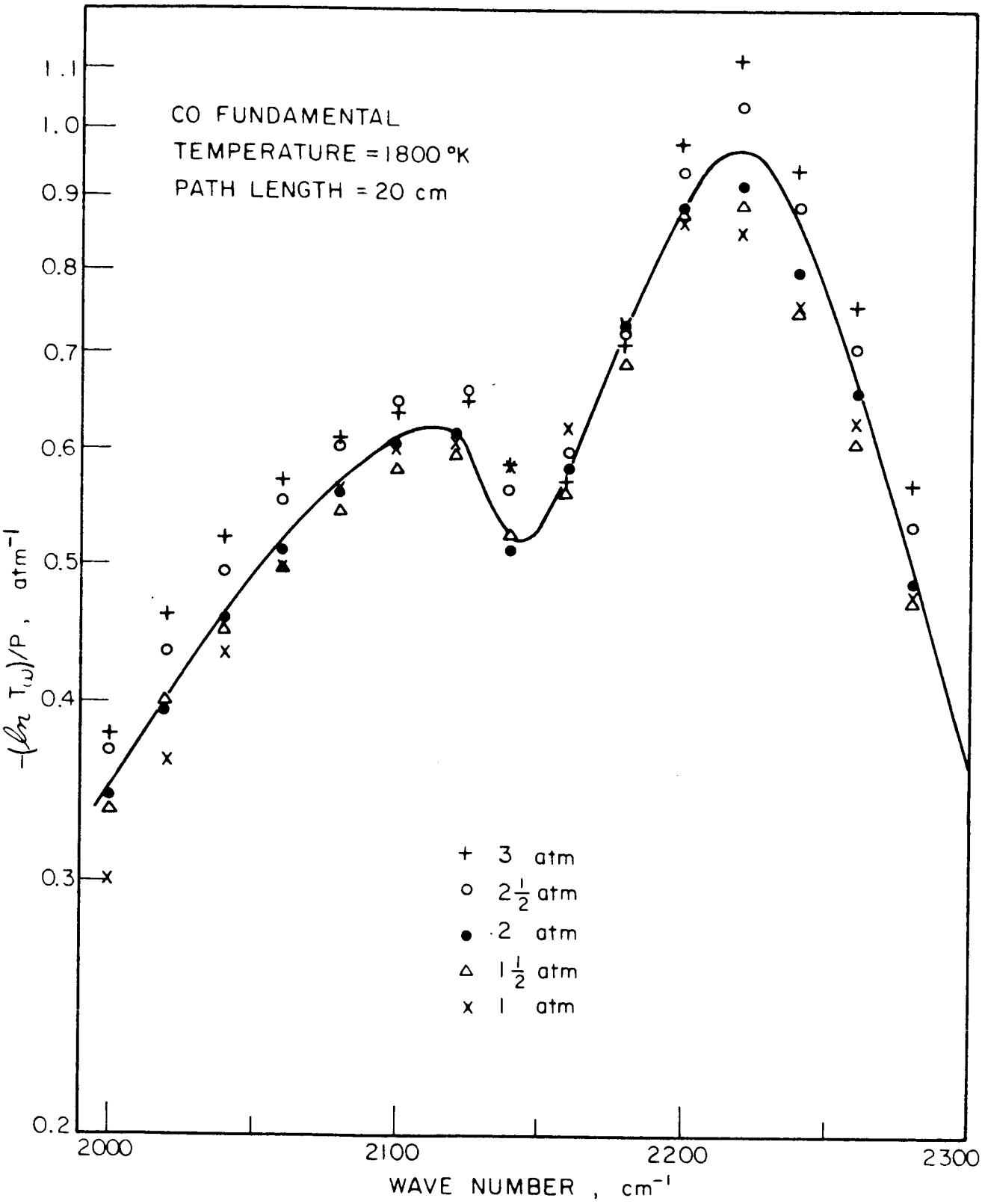

FIG. 19 SPECTRAL VALUES OF $-(\ln T_\omega)/P$ FOR CO FUNDAMENTAL AT TEMPERATURE 1800 °K AND PATH LENGTH 20 cm

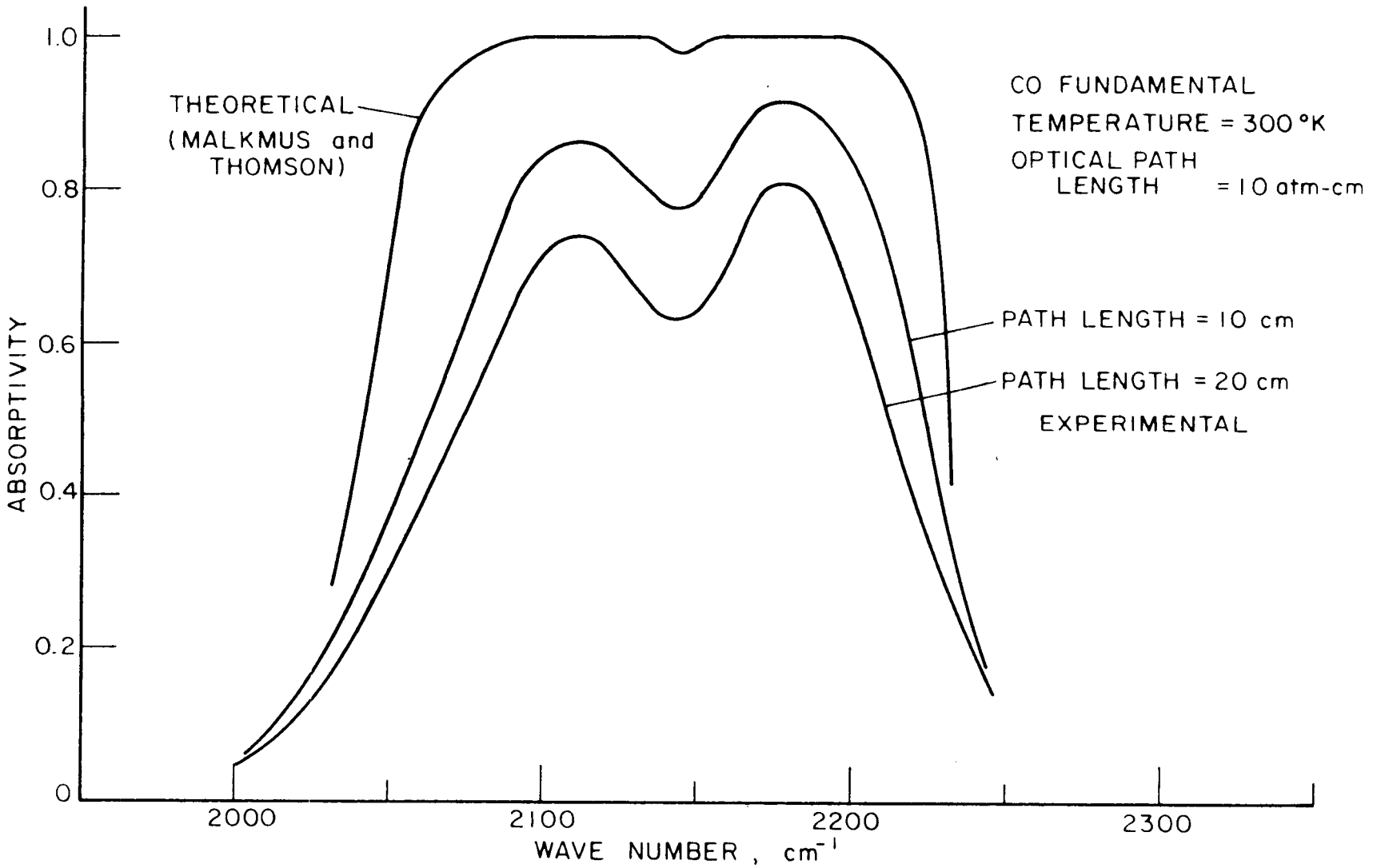

FIG. 20 COMPARISON OF EXPERIMENTAL RESULTS WITH THEORETICAL WEAK LINE APPROXIMATION AT TEMPERATURE 300 °K AND OPTICAL PATH LENGTH 10 ATM-CM.

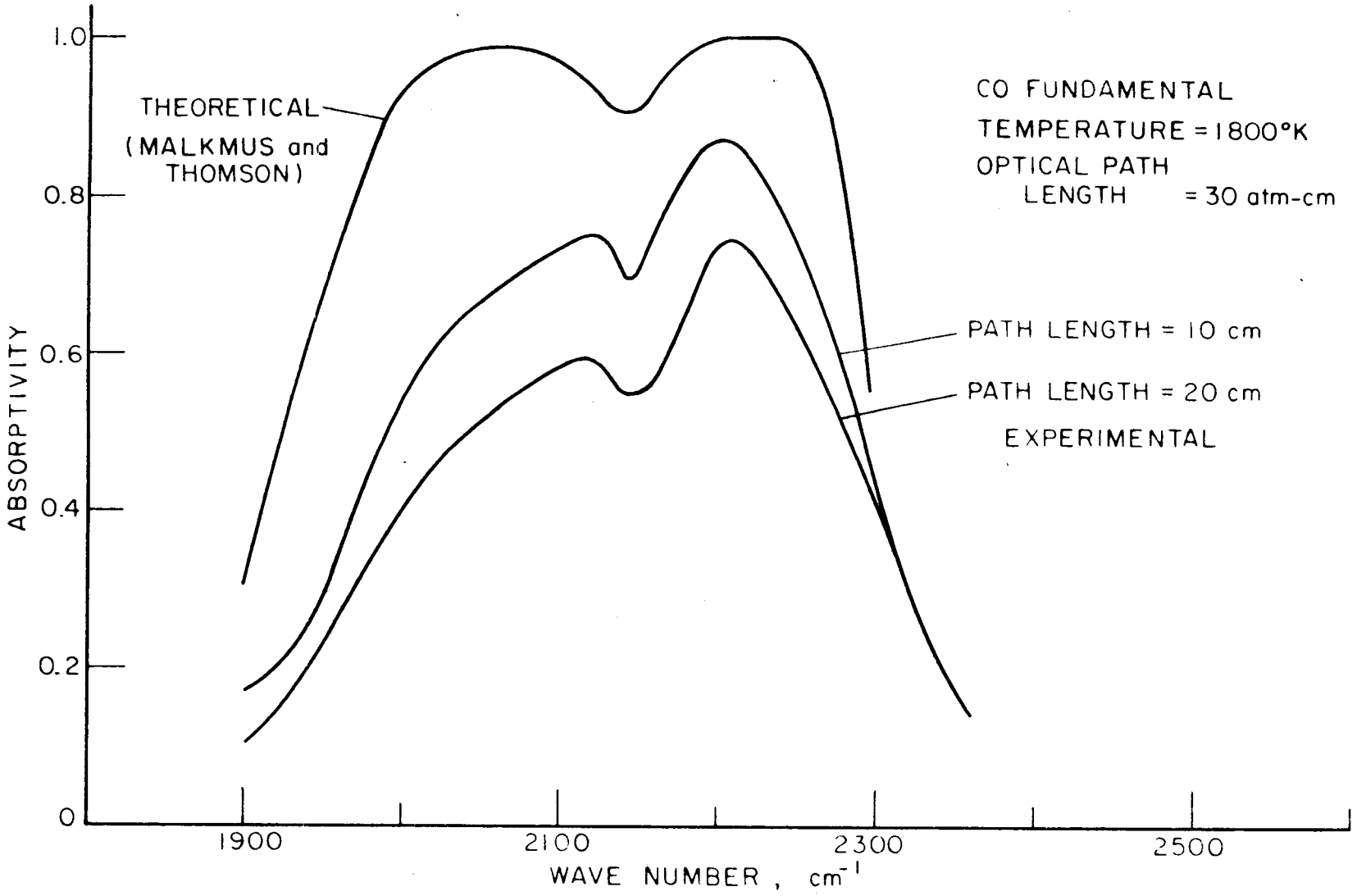

FIG. 21 COMPARISON OF EXPERIMENTAL RESULTS WITH THEORETICAL WEAK LINE APPROXIMATION AT TEMPERATURE 1800°K AND OPTICAL PATH LENGTH 30 ATM-CM.